Resistance of structures to explosion effects: Review report of testing methods

ERNCIP thematic area
Resistance of structures
to explosion effects
Deliverable D1

Kevin C., Ans van Doormaal, Christof Haberacker, Götz Hüsken, Martin Larcher, Arja Saarenheimo, George Solomos, Alexander Stolz, Laurent Thamie, Georgios Valsamos

December 2013

The research leading to these results has received funding from the European Union as part of the European Reference Network for Critical Infrastructure Protection project.

Report EUR 26449 EN

Joint
Research
Centre

European Commission
Joint Research Centre
Institute for the Protection and Security of the Citizen

Contact information
Naouma Kourti
Address: Joint Research Centre, Via Enrico Fermi 2749, TP 721, 21027 Ispra (VA), Italy
E-mail: ern-cip@jrc.ec.europa.eu
Tel.: +39 0332 78 6045
Fax: +39 0332 78 5469

http://ipsc.jrc.ec.europa.eu/?id=688
http://www.jrc.ec.europa.eu/

JRC87202
EUR 26449 EN
ISBN 978-92-79-35104-4
ISSN 1831-9424
doi:10.2788/57271

Luxembourg: Publications Office of the European Union, 2013

Printed in Italy

ERNCIP THEMATIC GROUP

Work package 1

Review report of testing methods

Thematic Group:

Resistance of structures to explosion effects

Coordinator: Dr Alexander Stolz, Fraunhofer Institute for High-Speed Dynamics, Ernst Mach Institute, EMI

Deputy Coordinator: Christof Haberacker, Bundeswehr Technical Centre for Protective and Special Technologies (WTD 52)

Editors:
Alexander Stolz
Christof Haberacker

Authors (in alphabetical order):
Kevin C.
Ans van Doormaal
Christof Haberacker
Götz Hüsken
Martin Larcher
Arja Saarenheimo
George Solomos
Alexander Stolz
Laurent Thamie
Georgios Valsamos

Acknowledgements:

The research leading to these results received funding from the European Union within the European Reference Network for the Critical Infrastructure Protection project hosted at the Joint Research Centre — European Commission — Via E. Fermi 2749 — Ispra (VA) Italy.

Abstract:

It is important to protect critical buildings (shopping centres, government buildings and embassies), infrastructure and utilities, train and underground stations against being damaged, destroyed or disrupted by deliberate acts of terrorism, criminal activity and malicious behaviour. Normal regulations and building guidelines do not generally take into account these threats. The introduction of regulations or guidelines should support the resilience of the buildings and infrastructure against explosive incidents.

In order to protect the infrastructure, methods are required to quantify the resistance of structural elements against explosive loading and to assess the hazards resulting from failure of an element. The applicable state-of-the-art techniques may be either experimental or numerical methods, or a combination of both.

Therefore, the thematic group (TG) on the resistance of structures to explosion effects was formed in order to bring the required expertise together, make it commonly available and to find and define harmonised methods and solutions which can be provided to the decision-makers responsible for critical infrastructure protection. This first report of the TG gives a comprehensive summary of the existing methods which can be used to analyse and test the resistance of glazing and windows under blast-loading conditions.

Within this context, the experimental methods of testing using high explosives and testing using blast simulators called shock tubes is presented and explained. In addition, the potential of numerical simulations is highlighted in terms of their applicability to the different glass materials.

A short, comprehensive theoretical background is given for each method. Based on this, each method is described with its requirements, realisation and the related measurement techniques. Furthermore, an interpretation of the measurements is highlighted.

For the numerical simulations, the basic discretisation and calculations schemes are presented in combination with the available constitutive material descriptions for the different significant materials. Finally the chances for verification and validation of the numerical results are presented.

Hence the report builds the basis for an actual evaluation of the different test methods and their applicability to certain problems, and provides helpful information for critical infrastructure stakeholders, owners and operators considering the structural resistance of the infrastructure to the effects of explosion in a comprehensive document.

Table of contents

1 Scenario definitions

In order to develop design-performance criteria, and subsequently test criteria, for blast-resistant glazing it is necessary to understand the threats to be considered, which are primarily from Improvised Explosive Devices (IED). There may also be a need to design blast-resistant glazing to protect from accidental gas or petrochemical explosions. However, in this case, the blast waves will have much lower pressures and longer durations than the blast waves from high-explosive events. Petrochemical explosions will not be considered further in this study.

Furthermore ideal field conditions are assumed in all explanations. Urban detonation scenarios may lead to different and more complex loading profiles. Possible amplifying or shading effects can be considered within the testing methods but require special expertise.

1.1 *Effects of high-explosive charges*

In an improvised explosive device (IED) explosion the terrorist initiates a detonator, containing a sensitive primary explosive, which produces a high-velocity shock wave which travels at supersonic speed through the main, secondary explosive charge causing a very rapid and stable chemical reaction. The speed is known as the detonation velocity and may be as high as 8000 m/s for high-grade military explosives. The detonation wave converts the explosive into very hot, high-pressure gases which cause a shock front in the air and continue to expand to support the blast wave.

There are a number of effects that are caused by the detonation of a high-explosive charge. These are:

Brisance. If an IED is detonated in contact with, or very close to a target, the high-velocity shock wave from the explosive will travel directly into the target, creating a shattering effect. The severity of this effect depends on the detonation velocity of the explosive, which is much higher for military-grade explosives than for improvised explosives.

Fire ball. The high-temperature gases arising from the detonation of an explosive form a fireball, which will last for a considerable time radiating heat and may cause heat damage or fires close to the explosion.

Air blast. As noted above, a blast wave is caused by the transmission of the shock wave from the explosive into the air and the subsequent expansion of the gases. It is the main way in which loads are applied to structures after an explosion. It is discussed in more detail in Section 2 below.

If an explosion takes place in the open and close to the ground, the shockwave will expand hemispherically. For internal explosions the shockwave will reflect off the walls, floor and ceiling. This occurs repeatedly with reduced intensity, creating a complex pressure field. If there are no openings which allow the gases to escape they will eventually reach a uniform and stable pressure. This is known as the quasi-static pressure (QSP).

Ground shock. If an IED is detonated close to the ground or a road surface the blast and brisance effects will cause a crater. The shock wave causing the formation of the crater will continue through the ground and is known as ground shock.

Primary fragments are parts of the IED that are driven at high velocity by the brisance effect. They may be parts of the container (e.g. the vehicle) or deliberately added fragments (e.g. ball bearings).

Secondary fragmentation may result from objects external to the IED being propelled by the blast wave and the high gas pressures. Such objects may be either building debris caused by the blast wave or loose items, such as gravel.

It is not practicable to specify glass to resist the brisance caused by a contact explosion so this effect will not be considered further. The effects of fire balls and ground shock are not likely to affect glazing.

At relatively close ranges there will be a combined effect of blast loads and impact by primary fragments.

Data on primary fragments from personnel-borne IEDs (PBIEDs) and vehicle-borne IEDs (VBIEDs) carries security classifications. However it would be possible to develop representative fragments to carry out ballistic testing following similar test procedures to those for bullet-resistant glass in EN 1063. If the IED is close to the target, the target will experience the combined effects of fragment impacts and blast loading. This is an extremely complex problem which still needs considerable research.

By its nature, secondary fragmentation is widely varied and it is not considered possible to characterise it for the development of test procedures. The effects of primary and secondary fragments will not be considered further in this study.

1.2 TNT Equivalence

There is considerable variation in the effectiveness of different explosives. The difference in performance may be due to chemistry or to the efficiency of the manufacturing process. The latter is particularly significant for home-made explosives, which have been used frequently by terrorists. It is convenient to compare the relative effectiveness of an explosive to a reference explosive.

The conventional practice is to use TNT (Tri-nitro-toluene) for this purpose and to compare the explosive mass to the mass of TNT needed to produce the same effect. Hence a charge may be defined as being equivalent to a certain mass of TNT in kg.

An explosive can also be defined as having a TNT equivalence which is a ratio of its effect. If the equivalence is greater than unity the explosive is more powerful than TNT. It should be noted that the TNT equivalence is likely to differ depending on the effect being considered — these are usually either the peak pressure or the impulse, although an average value is often used. Table B-1 in (ISO 16933), Table 2.6 in (Conrath, et al.) and (Maienschein, 2002) provide TNT equivalences for a number of commonly used explosives.

The blast field close to the charge is affected significantly by the shape of the charge. To ensure that the blast wave propagation is consistent the above-ground charges should be spherical to initiate spherical propagation. Similarly charges on the ground should be hemispherical.

1.3 Improvised explosive devices (IED)

Unlike conventional military weapons, which can be closely defined, terrorist IEDs are likely to be very varied in explosive type, quality and charge size. It is convenient to subdivide the IEDs into vehicle-borne IEDs (VBIED) and personnel-borne IEDs (PBIED). Typically VBIEDs may contain as much as a few hundred kilograms of explosives whilst PBIEDs, as they have to be carried, will not contain more than a few tens of kilograms. For the purposes of explosive effects it makes little difference whether the IEDs are delivered or used as suicide devices.

1.4 IED Location

The location of an IED relative to the target is crucial as blast effects from an external explosion diminish very rapidly with distance and the effects of an internal explosion are magnified as the blast is confined.

For IEDs used against buildings there are four broad scenarios:

- **Internal explosions** — glazing in buildings will rarely withstand the effects of an internal explosion. This situation will not be considered further in this study.
- **Contact explosions** — as glazing will not withstand contact explosions this situation will not be considered further in this study.
- **Near field (or close-in) explosions** — this is only likely to be relevant for PBIEDs, as a VBIED at close range is likely to have a devastating effect on most buildings.
- **Far-field (or blast) explosions** — PBIEDs are likely to be relatively ineffective as the range increases and VBIEDs are likely to be the dominant concern.

Hence this study will consider only near-field explosions for PBIEDs and far-field explosions for VBIEDs and is first focused on glass components.

1.5 IED threats

The predominant threat criteria are the charge mass and the range (stand-off distance) from the IED to the target. Both criteria are infinitely variable and fundamentally uncertain as both are chosen by the terrorist and are therefore outside the control of the building owner. In addition it may be unaffordable to PROTECT the building and only practicable to MITIGATE the effects of potential terrorist attacks. Depending on the geometrical situation around the protected building the stand-off distance can be increased by using several architectural and urban planning measures (Gebbeken et al., 2012).

Therefore, there is a need to have agreed threat levels so that designers can agree with building owners the level of mitigation that is to be achieved. This will also facilitate the development of suitable suites of windows by manufacturers and assist test houses in developing consistent test conditions. This philosophy is reflected by the current CEN and ISO standards for blast-resistant glazing and NATO STANAG 2280, all of which provide matrices of charge masses and ranges (cf. section 1.6). However these matrices vary in the spread of charge masses and ranges specified.

1.6 List of references

CEN, 2001. EN 13123-1: Windows, Doors and Shutters — Explosion Resistance — Requirements and classification — Part 1: Shock Tube.

CEN, 2001. EN 13123-2: Windows, Doors and Shutters — Explosion Resistance — Requirements and classification — Part 2: Range test.

CEN, 2001. EN 13124-2: Windows, Doors and Shutters — Explosion Resistance — Test Method — Part 1: Shock Tube.

CEN, 2001. EN 13124-2: Windows, Doors and Shutters — Explosion Resistance — Test Method — Part 2: Range test.

CEN, 2000. EN 13541: Glass in building — Security glazing — Testing and classification of resistance against explosion pressure.

ISO 16934: 2007 Glass in Building — Explosion-resistant Security Glazing — Test and Classification by Shock-tube Loading.

ISO 16933:2007/Cor1:2008 Glass in building — Explosion-resistant security glazing — Test and classification for arena air-blast loading.

CEN, 1999. EN 1063: Glass in building - Security glazing - Testing and classification of resistance against bullet attack.

Conrath E.J, Krauthammer T, Marchand K.A, Mlakar P.F, 1999. Structural Design for Physical Security: State of the Practice, SEI American Society of Civil Engineers.

Maienschein J.L 2002. Estimating Equivalency of Explosives through a Thermochemical Approach, preprint UCRL-JC-147683, Lawrence Livermore Laboratory, Berkeley.

Gebbeken N, Döge T, Larcher M, 2012. Safety and Security of Urban Areas through Innovative Architectural and Structural Concepts, Proceedings 7th Security Research Conference Future Security Sept. 4-6, 2012, Bonn, Germany.

NATO 2008, STANAG 2280 Ed.1, Design Threat Levels And Handover Procedures For Temporary Protective Structures.

2 Shock waves

2.1 Properties of shock waves

From the physical point of view waves are a kind of energy spread. Depending on the amplitude and the shape of the wave-profile, as well as the response of the medium in which the wave propagates, a distinction between elastic and plastic waves has to be made. Generally speaking, shock waves are strong compression waves which are, for instance, caused by the high-speed burning processes coming from detonations. The spread of these waves in unobstructed free space is three-dimensional. With increasing distance from the detonation centre, the pressure decreases rapidly.

2.1.1 Sources and characteristics of shock waves

Scenarios which are characterised by shock-wave loading are explosions, bursting vessels or high-speed impact events. In explosions, shock waves come from the high energy released due to the burning processes of high explosives or from the explosion of gas-air mixtures. However, only high-speed burning processes can cause shock waves. These are called detonations. Such strong compression waves can come from different explosive sources, such as high explosives (TNT, C4), gas-explosions (hydrogen-air mix) or burst pressure vessels (Gebbeken et al., 2012). Solid explosives and reactive gaseous mixtures are often transformed by detonations to blast waves with high amplitudes. Compression waves at a large distance from the source show qualitatively identical characteristics, with no dependence on the scenario (Sauer et al.). In cases of contact detonations and close-in detonation, the characteristics of compression waves can differ strongly.

Shock waves are characterised by a compression phase (positive phase) with a very high peak pressure and a following undertow phase (negative phase). The compression phase starts with a shock front. It shows a strong increase in the pressure from the ambient pressure (p_0) to the peak pressure within a timescale of nanoseconds. Figure 1 shows a simplified form of the pressure-time history of a shock wave, and indicates the relevant parameters.

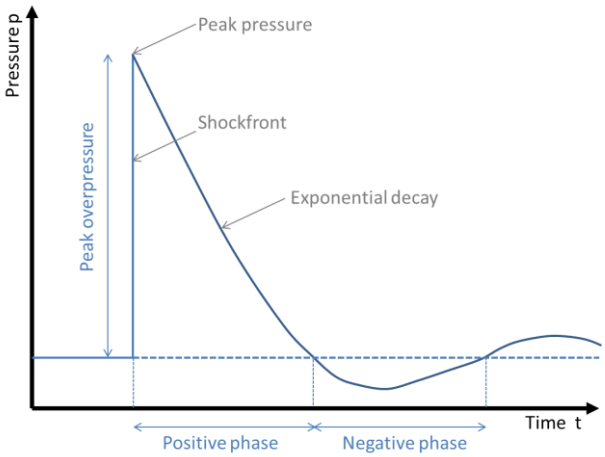

Figure 1: Simplified sketch of a blast wave with its characteristic properties

Explosions are distinguished by the speed of the burn-off process. In the case of a *detonation* the burn-off of the high explosive occurs with a velocity above sound speed in the explosive, while the burn-off velocity of a *deflagration* is below it. The propagation of the shock wave in the air outside the explosive material is called a blast wave. Ideally blast waves spread spherically unless there are obstacles, which cause reflections.

With an increasing distance between the loaded structure and the explosion source the shock wave becomes close to plane. This results in a quasi-plane load, characterised through a specific pressure-time history at any point on the structure.

When a shock wave hits a structure, reflection occurs, which is described by the reflection coefficient c_r :

$$c_r = \frac{p_{ref}}{p_{inc}} \tag{2.1-1}$$

with p_{ref} being the reflected pressure and p_{inc} the incident pressure, respectively.

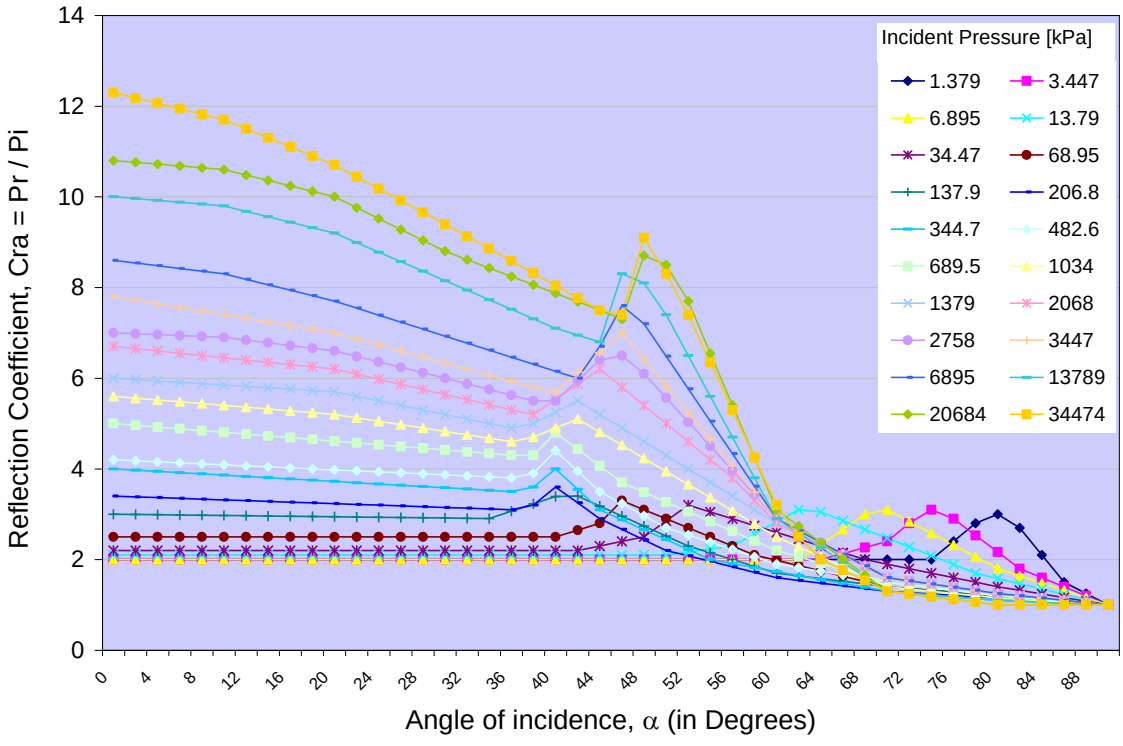

Figure 2: Behaviour of c_r versus the angle of incidence and magnitude of incident pressure according to UFC (UFC, 2008)

The reflection coefficient c_r compares the amplitudes of the reflected wave and the incident wave. It is itself a function of the incident overpressure and also the angle of incidence (Fig. 2). For surfaces parallel to the direction of propagation (angle of incidence 90°), the reflected pressure is equal to incident pressure, therefore also called side-on pressure.

The peak overpressure of the reflected wave defines the load on the structure. As shown in Figure 2, this pressure is higher than the peak pressure of the incident wave. This phenomenon is caused by the fact that air molecules adjacent to the structure are unable to move freely (Gebbeken et al., 2012).

An example of a shock wave is given in Figure 3. A comparison of the reflected pressure (black curve) to the side-on pressure (red curve) is shown. The example represents a shock-tube test on a glazing element.

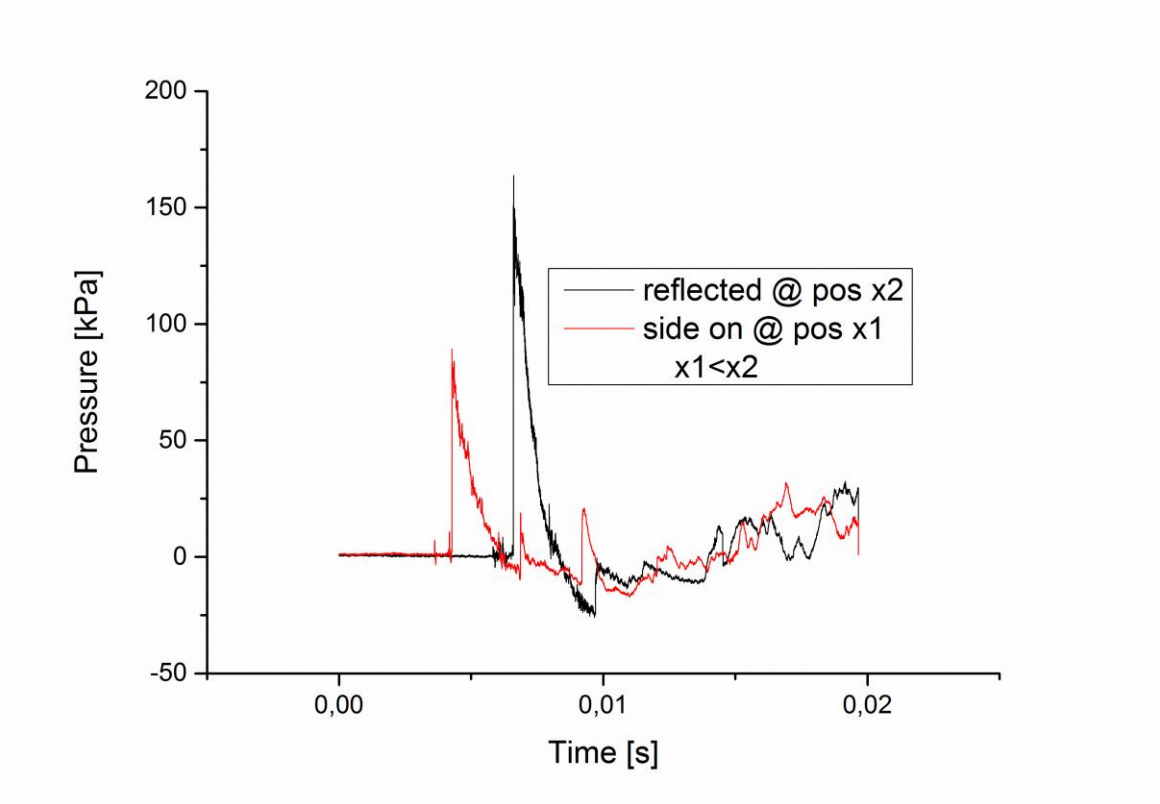

Figure 3: Comparison of pressure-time histories of the reflected and the side-on pressure during a shock-tube test on a glazing structure

2.1.2 Formation of shock waves

Shock waves differ strongly from linear elastic waves regarding their expansion and propagation (*Riedel*, 2004). Very high-pressure amplitudes carry the material into the non-linear, plastic region of the pressure-density curve (Figure 4, left). Since the propagation velocity of the wave depends on the gradient of this curve, the wave's peak propagates faster than its leading and trailing edges, leading to the formation of a steep shock front (Figure 4, right), characterised by a discontinuity in pressure and density.

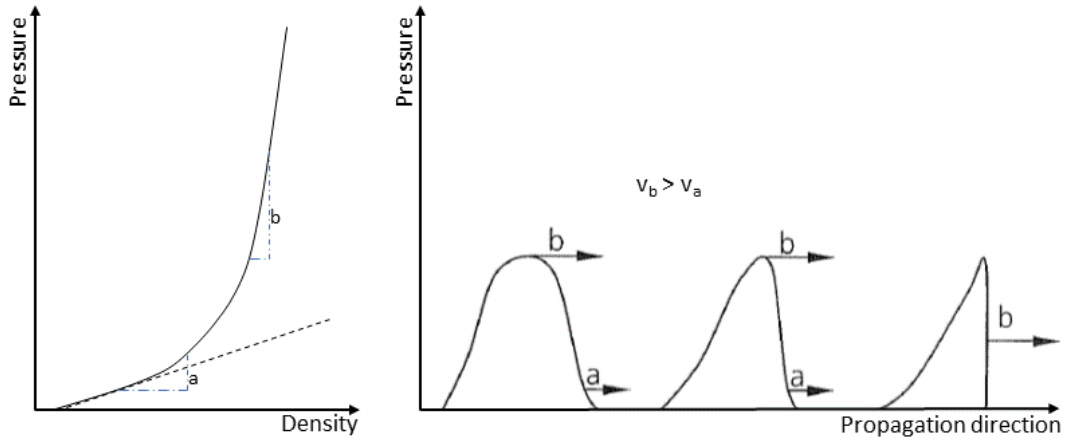

Figure 4: Left: pressure-density relation, right: formation of a shock front (Riedel et al., 2010)

2.1.3 Loading scenarios of shock waves

The highest pressures occur at a close range of the detonation source. As distance increases from the detonation origin the pressure reduces strongly. The peak pressure in the contact scenario detonation reaches a value of several GPa for a very short duration (micro-seconds). Air blast from detonations with a large standoff between source and structure leads to strongly reduced pressures (kPa) and loading durations of milliseconds. Because of this there is a distinction between the loading scenarios.

A classification of the detonative scenario is possible through application of the scaled distance Z defined as

$$Z = \frac{R}{\sqrt[3]{W}} \qquad (2.1\text{-}2)$$

R is the distance [m] from the detonation source to the loaded structure and *W* the charge mass [kg]. According to (Riedel et al., 2010), Table 1 summarises some loading classification scenarios and the corresponding scaled distances for reinforced concrete and lightweight structures.

A distinction between different loading scenarios is required, because different effects and damage can occur on the loaded structure. Contact detonations are characterised through high pressures, which load a structure for just microseconds. The effects on the structure are local. Shear and punching failure is activated leading, depending on the strength and the ductility of the loaded material, to fragmentation on both the loaded side and the rear side of the structure.

Table 1: Distinction of the detonation scenario through the scaled distance Z according to Riedel, et al., 2010

Loaded structure	Scaled distance Z	Scenario
Reinforced concrete structures	Z < 0.5	Close-in
	Z > = 0.5	Blast
Lightweight structures	Z < 2-6 *	Contact detonation
	Z > = 2-6 *	Blast

* Due to the broad range of lightweight structures and their specific dimensions only a range and not a precise value can be given

Blast loads lead to large- or full-area loading of the involved structure. The pressures are significantly lower, resulting in lesser damage. This results in a global structural response, for example damage through bending (Riedel, 2004). Due to the strongly reduced pressures (some hundred kPa in some tens of milliseconds) fragmentation is not expected in structures exceeding a certain strength and stiffness. It can be seen that the dynamic loading of structural elements by high explosives is dominated by charge weight and the distances between detonation source and member. The effects of the different scenarios to the structural behaviour are broadly outlined in Tables 1 and 2.

Table 2: Comparison of explosion scenarios depending on the distance between source and structure regarding pressure, strain rates and type of damage.

Scenario	Pressure [MPa]	Strain rate [s^{-1}]	Damage
Contact detonation	5000	10^4 …10^6	Local
Close-in detonation	500	10^2 …10^4	Local / global
Blast	1	10^{-2} …10^1	Global

Experimental methods aid in the investigation of the structural response of building elements. The effects of a detonation over a large distance (blast loading) can be analysed through shock-tube tests or with detonative experiments. The next section of this chapter will give detailed explanations.

Figure 5 presents a pressure-time history of a shock-tube test on a glazing element. A large timescale of 250 ms is documented. Beside the strong pulse at the beginning, which is characterised through a shock front, lots of reflections, however with significantly lower amplitudes, are visible. These

reflections occur due to reflection of the loading wave in the shock-tube and represent a complex blast load. Such a scenario occurs if the blast wave is reflected by more than one obstacle in the environment of the investigated structure.

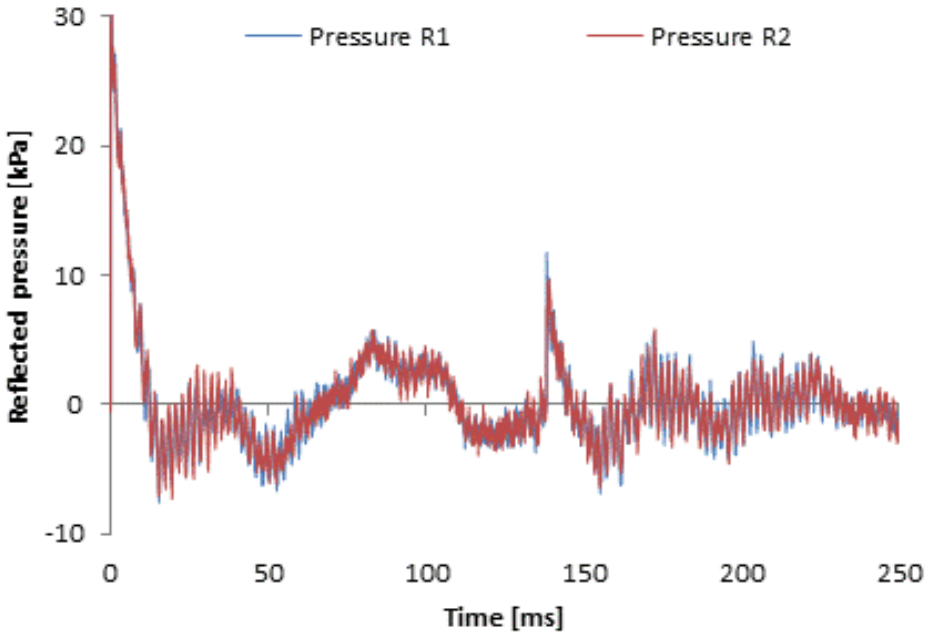

Figure 5: Pressure-time history as reflected pressure measured on a glazing structure for an experimental time of 250 ms

Figure 6 shows a realistic blast wave through a pressure-time history measured on a glazing element due to a shock-tube test. The timescale is about 70 ms, much shorter than that of Figure 5. Here the typical characteristics of a shock wave become visible. The blast load is characterised through a shock front at the beginning of the load followed by an exponential decay within the positive phase followed by the negative phase. The high-frequency oscillations, shown in the pressure-time history, result from the high eigenfrequency of the used pressure sensor. Furthermore, the sampling rate chosen is very high in order to get high-precision results.

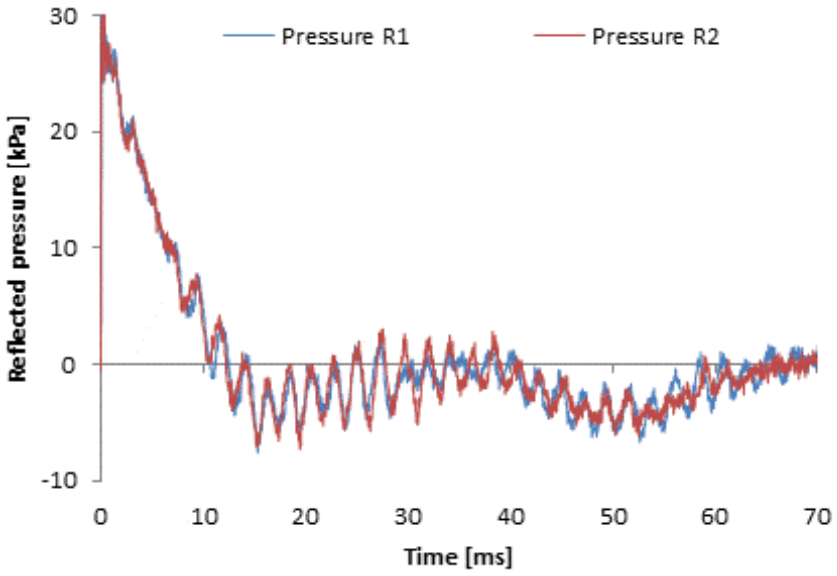

Figure 6: Pressure-time history as reflected pressure measured on a glazing structure for the first 70 ms of the experiment after loading

2.1.4 Characterisation of shock waves in standards

European and international standards recently started to provide a classification for the 'explosion effect restraint' of glazing structures, windows and doors. For example the European standard EN13123-1 defines a typical pressure-time history of a blast load, which should be realised in classification tests with shock-tubes and free-field detonations (CEN). Figure 7 represents the suggested pressure-time history. When compared to the real blast (Figure 6) the simplified model shows strong accordance.

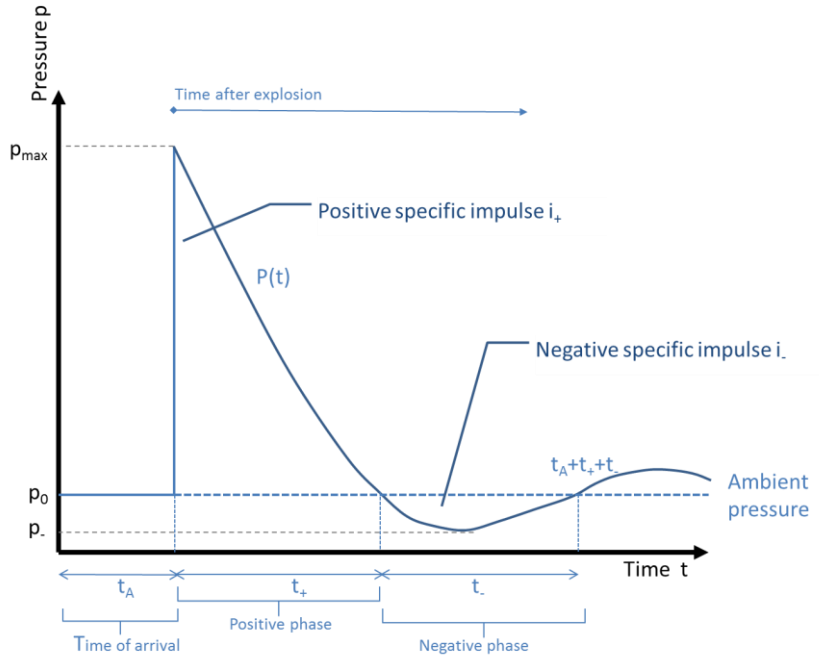

Figure 7: Description of a blast wave as an ideal pressure-time history according to the European standard EN 13123-1

2.2 Formation and propagation of shock waves

Two fundamental methods exist for experimentally determining the effects of blast and shock on a target system. These methods differ primarily in the choice of the simulator facility used to generate the test environment. The experimenter must generally choose to use either a shock-tube or a high-explosive (HE) event as the source of the test environment. While making this choice, the simulator's characteristics should be kept in mind. This chapter explains the principal functionality of these two classes of simulators for blast trials.

2.2.1 Shock waves caused by high explosives

Full-scale arena tests using high explosives are conducted to evaluate the performance of structural members and building components against blast loads. One or more test samples are placed at suitable distances from the charge on a level area with no obstacles. The test samples should be placed in robust cubicles to ensure that the behaviour of the test sample is not modified by the effects of the blast wave loading the back of the sample. A number of standards have been developed for testing windows and glazing with high explosives in an arena test (cf. CEN and ISO, 2008).

Ideally the test arena should be surfaced with concrete, asphalt or cement-bound soils. This facilitates placing the charge and test samples and reduces the risk of the target being damaged by secondary fragmentation. It also ensures that the amount of energy absorbed in cratering is minimised and the test approaches the hemispherical surface burst condition of the Kingery-Bulmash air blast curves (Kinney et al., 1985). The smooth surface also reduces the turbulence caused by any surface irregularities or vegetation.

For larger charges, representing VBIEDs, the charge is usually raised to represent it being mounted in a vehicle. This has the useful benefit of reducing the damage to the surface of the test arena. The charge is formed into a sphere and placed on a support made of frangible material e.g. polystyrene foam (Figure 8). As the charge is slightly raised it represents an air burst at very low altitude and there will be a ground reflection from the shock wave which will catch up with the direct wave front forming a Mach Stem wave front. For the ranges that are usually considered, unless the target is unusually tall the Mach Stem wave will be taller than the test sample. Similarly, unless the target is unusually broad, the spherical shock front will effectively be a plane wave by the time it reaches the target. In practice the assumption that the charge is a hemispherical surface burst gives a close approximation.

Figure 8: Typical arena test set-up for rating window systems.

For PBIEDs, representing small, carried charges such as briefcase bombs, the charge is usually placed on the ground. In this case, there are no (separate) ground reflections and a Mach Stem wave front is not formed. However the range will be fairly short so the pressure applied to the glazing sample will be non-uniform as the shock front will still be spherical.

It is not possible to directly measure the pressure on the glass sample. It has been found that the pressure gauges mounted in the steel cubicles that are usually used may give unsatisfactory readings due to vibrations in the steel. Instead a group of three pressure sensors is mounted in a concrete gauge block which has the same frontal dimensions as the cubicle and is placed at the same range. The centre of the gauge group is placed to represent the centre of the test sample. Alternatively, if the gauges are mounted on the cubicle adjacent to the sample it will be necessary to carry out calculations to establish the pressures actually experienced by the sample.

The test cubicle is clearly much smaller than the building in which windows will be used and the blast wave will clear the cubicle more quickly than it would clear the building. At the same range both will experience the same peak pressure but the test sample in the cubicle will receive a reduced impulse due to the clearing effects. Consequently there is a need to adjust the charge weight and range to obtain the correct pressure and impulse values. A common, and conservative, approach is to reduce the range so that the impulse is correct but this will result in increasing the pressure acting on the

test sample. It is also possible to increase the impulse experienced by the sample by extending the size of the reflecting surface of the test cubicle, thus reducing the effects of clearing.

In a high-explosive arena test it is economical to place a number of target cubicles and gauge blocks round the charge. In this case it is important to ensure that the blast flowing around the cubicles does not affect the blast pressures experienced by adjacent cubicles. Model studies and site experience show that the effect is minimal if the clear space between cubicles and gauge blocks at the same range is at least one cubicle width. For cubicles at different ranges, the rear cubicle should be placed outside a line drawn at 45° from the front corner of the front cubicle. A sketch of a typical test set-up is shown in Figure 9:

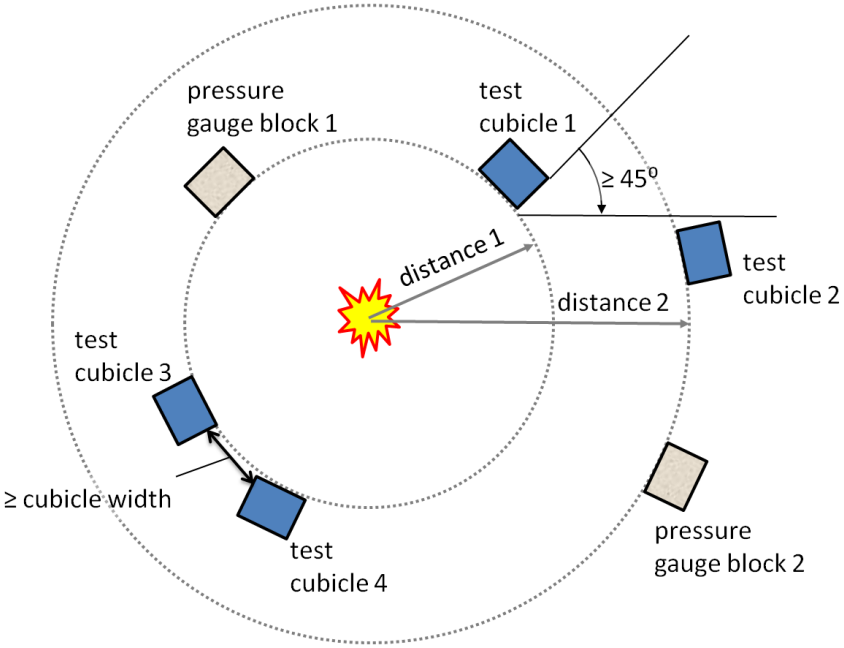

Figure 9: Typical arena test set-up

Studies have also assessed the inaccuracies that may occur due to the test cubicles not being normal to the radius from the charge. It was found that variations in the blast pressure and impulse due to misalignments of less than 5° were negligible (see Figure 2).

In a high explosive test it is possible to test very large test samples such as sections of buildings or large sections of glazed facades. In such cases it is important to consider the effects of the Mach Stem wave front and the assumption that the shock wave approximates a plane wave.

2.2.2 Shock waves in shock tubes

The second method for analysing blast loads is through shock-tube tests. The accomplishment of shock-tube tests is an upcoming method, because it is possible to test loadings with high accuracy and with high reproducibility. Through the generation of a shock wave an idealised one-dimensional part of a detonation wave is simulated with shock-tube tests. The load on the structure is characterised through a uniform pressure-time history on the whole structure, as shown in Figure 10.

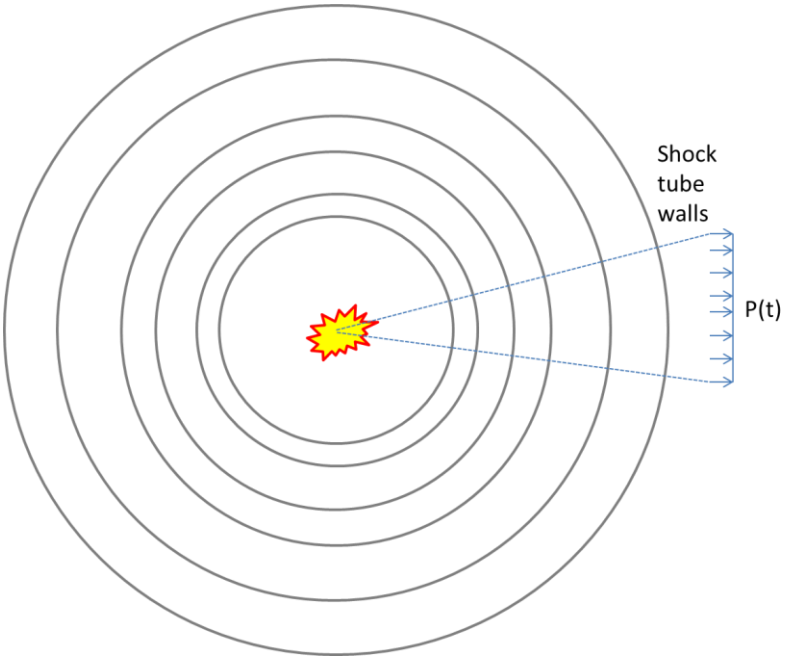

Figure 10: Propagation of a shock wave due to detonation and portion simulated through a shock tube

2.2.2.1 Shock tubes operated by explosives

The most elementary device for producing an air shock wave is a simple, constant-area shock tube. To generate the blast loading an explosive charge is placed at the end. When the explosive charge detonates a hemispherical shock front is formed. As soon as the shock front impinges on the walls of the tube it becomes more and more even. After about five tube diameters, the shock front has formed an approximately flat plane except for a small deflection in a thin layer next to the inner surface (Figure 11).

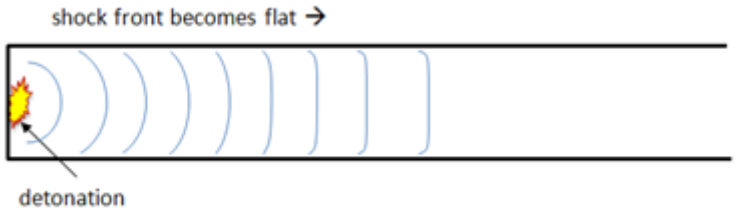

Figure 11: Propagation of a shock front in a tunnel

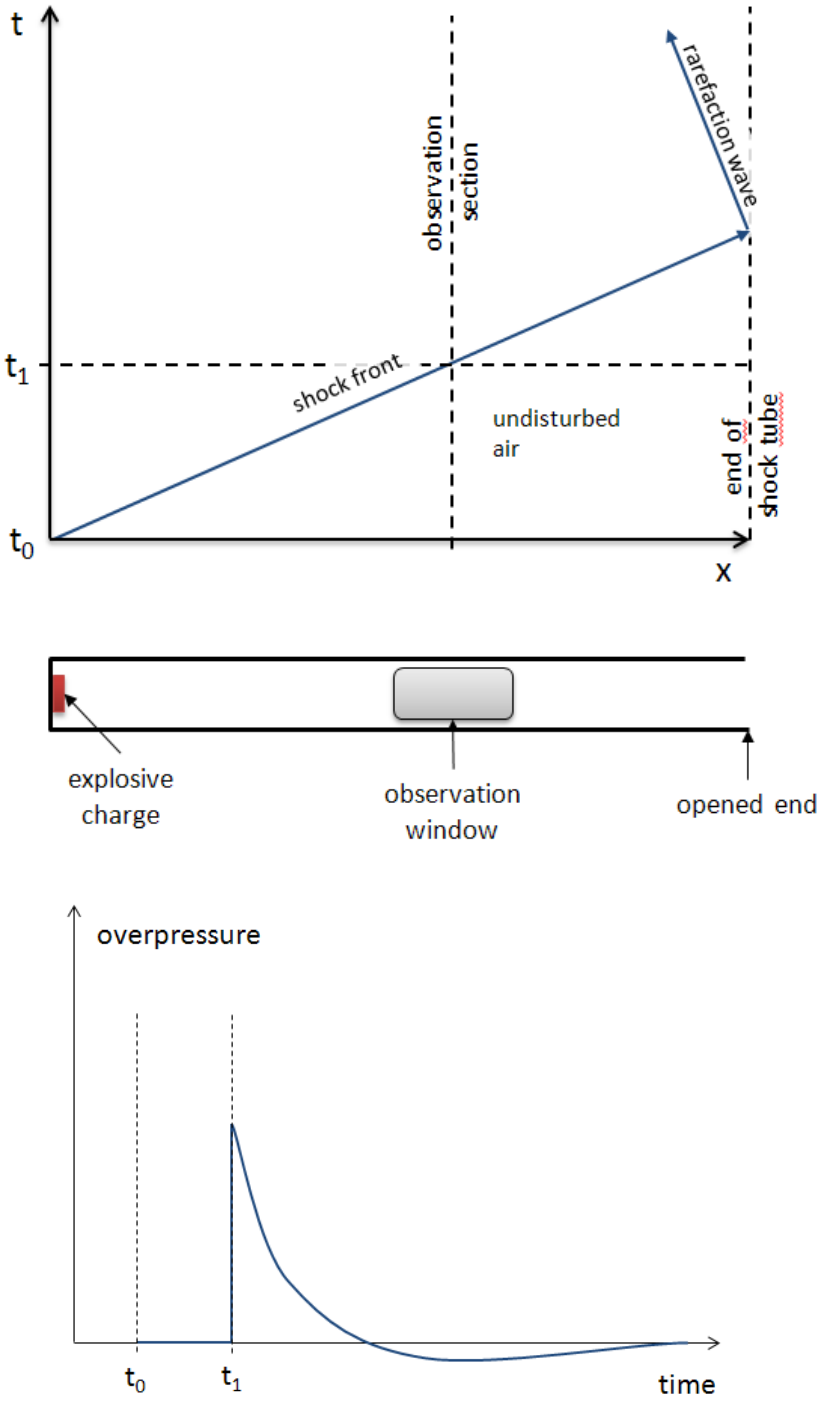

Figure 12: Propagation of a shock front in a shock tube operated by explosives

While travelling along the tunnel, the pressure curve steepens (Figure 6, right). After a certain distance the curve has the typical shape of a blast wave. At this distance one can imagine an observation window which is, as a result of this, in the optimal section for test equipment (cf. Figure **12**). If one measures the pressure-time history in the observation window, one would see a typical blast wave form as idealised in the lower part of Figure 12. Figure 12 also illustrates the time-path diagram of the travelling shock front.

When the shock wave arrives at the open end of the shock tube, a rarefaction wave is created, which travels back upstream. This rarefaction wave accelerates the out-flowing gas, and thereby causes its pressure to also drop below the ambient pressure. This low-pressure area then gives rise to a refilling process, which results in an oscillating airflow in and out of the tube. In the example shown in Figure 12 the rarefaction wave is yet to have any influence on the observation section. The rate at which the pressure decreases, and the occurrence of a negative phase, depends on the specifications of the open end and the whole design of the shock tube.

If a free field explosive event is to be simulated in a shock tube, far less explosive mass is needed. For example a scenario with 1,000 kg TNT-equivalent at a distance of 80 m can be reproduced with 425 g TNT in a shock tube with a diameter of 2 m.

In reality there is a wide variety of shock-tube configurations. For example, some shock tubes have a conical widening and are closed at the end. However, the principal effects can be demonstrated in a few ideal cases that are shown in the following illustrations.

If the shock tube is closed at the end of the driven section, the shock wave will travel back and forth from one end of the tube to the other (Figure 13). Most closed-ended shock tubes are limited in size to a target dimension of about 3 m. Some open-ended shock tubes are larger but targets will need to be mounted in cubicles and subjected to clearing effects.

What follows is a series of peaks until a static pressure is reached. Due to the larger amount of gas inside the shock tube the static pressure is higher than it was before the explosion. The amplitude and the location of the reflection depend on the mass of the explosive, the shock tube cross-section and the distance to the test object and the walls. In the example in Figure 13 the first reflection occurs at t_2, visible as a second, smaller peak.

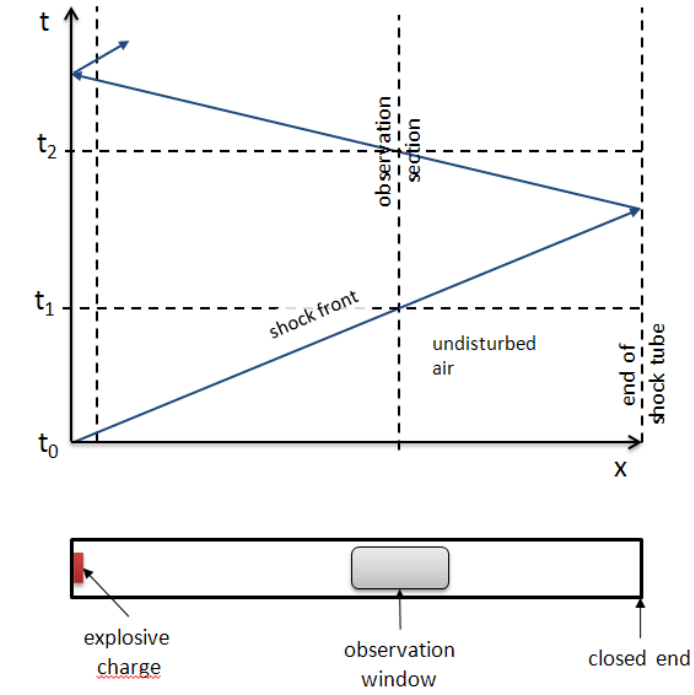

Figure 13: Propagation of a shock front in a closed shock tube

Figure 14 shows a real-life recording of the pressure in a shock tube with various reflections. The secondary y-axis shows the impulse (red curve).

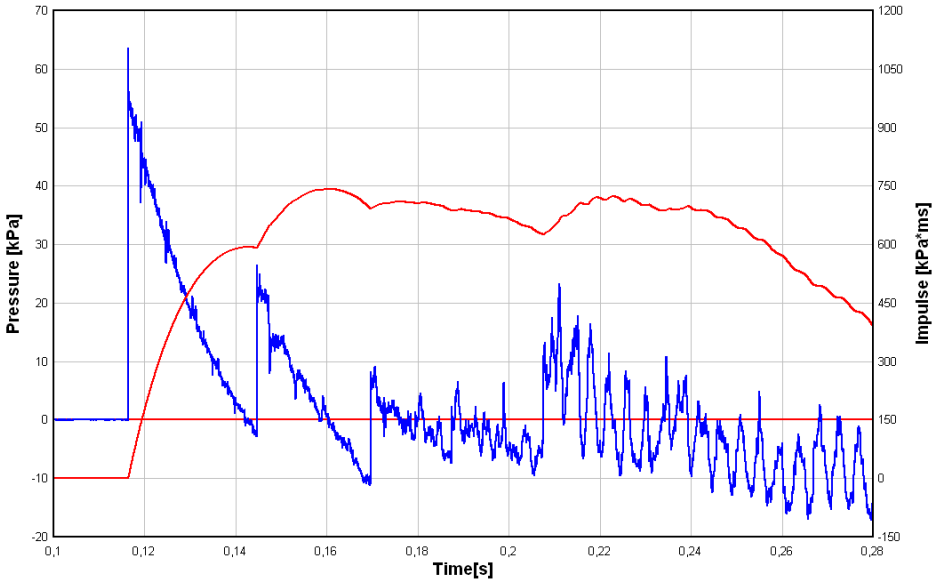

Figure 14: Realistic pressure function with reflections

To simulate the whole blast wave profile of very high-explosive charges as closely as possible, the reproduction of a negative phase might also be required. In this case specific blast tunnels evolved from shock tubes can provide approximately realistic pressure functions. An example for a type of construction can be found in the STANAG 4524.

2.2.2.2 Shock tubes operated by compressed gas

Apart from explosive-operated shock tubes it is equally common to use compressed gas as the driver. In its simplest form, a compressed gas-driven shock tube consists of a tube with a constant cross-section which is divided into two sections by a diaphragm. In some cases there may be also a conical expansion section.

Both sections are filled with gases under different conditions. Initially the gases are at rest in both chambers. As a convention for shock tubes and tunnels, the left section is called the driver or high-pressure section, containing the driver gas and the right part is called the driven or low-pressure section or the expansion chamber, containing the driven gas (see Figure 15 in the middle).

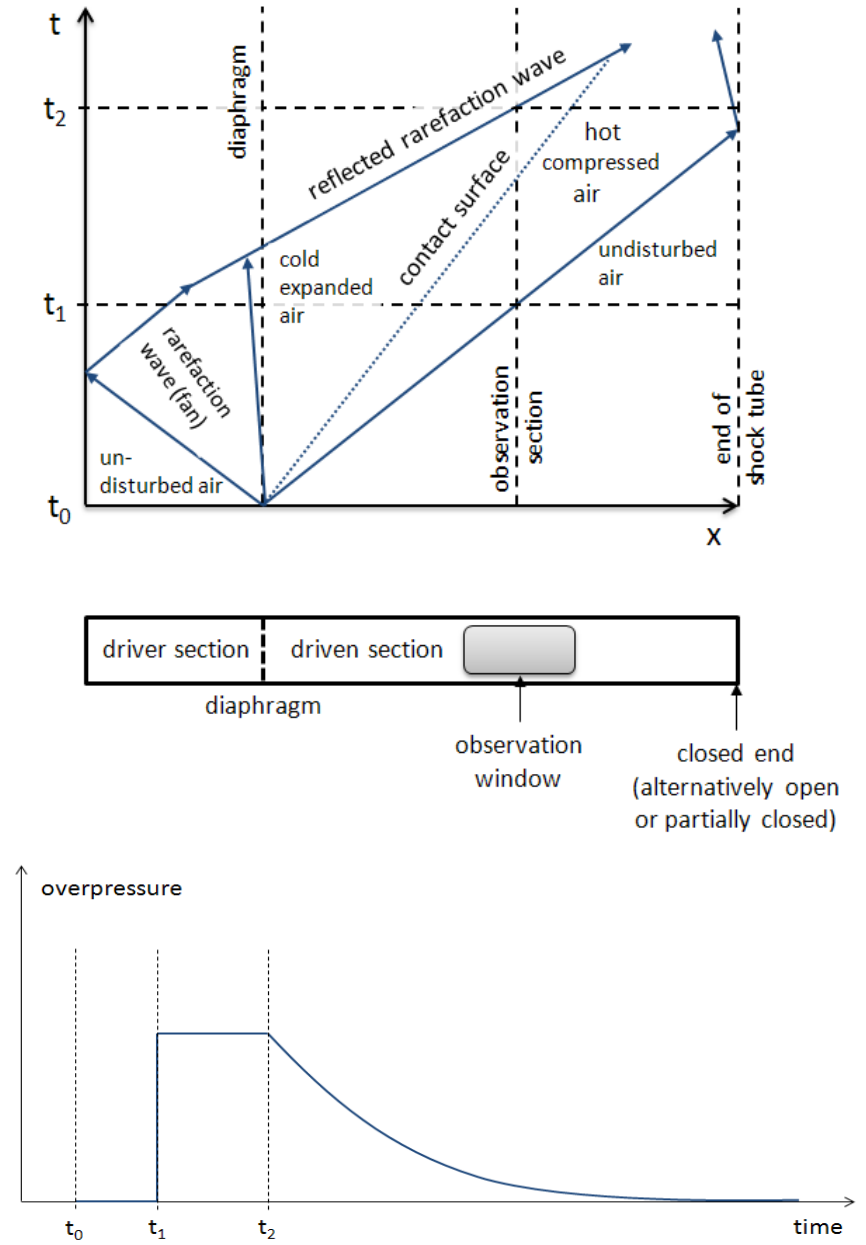

Figure 15: Theoretical flat-topped overpressure decay in the observation section of a simple shock

After rupturing the diaphragm the pressure starts to even out by producing a compression wave which expands into the driven section and a rarefaction wave which travels at the speed of sound into the driver section. Both waves are indicated in the time-path diagram in Figure 15. The compression wave steepens into a shock front (Figure 15, at t_1), whose peak static overpressure depends essentially on the initial pressure and the speed of sound differential across the membrane.

The driver gas cools on expansion, creating a discontinuity, called the contact surface (t-x diagram in Figure 15), between the driver and the driven gas. The velocity and pressure are constant across this surface, but the density, temperature, and hence the speed of sound, are not. This surface can be avoided by enhancing the speed of sound in the driver gas. This measure, which also increases the peak static overpressure, can be achieved by heating the driver gas to an appropriate temperature, or by adding a gas at higher sound speed.

The time history of the shock wave is greatly influenced by the discharge rate of the gas out of the driver section. This rate stays constant until the initial rarefaction wave, after having reflected at the closed end of the driver, enters the driven section. This event marks the end of the period of constant flow. In the observation window in Figure 15 the period of constant flow ends when the rarefaction wave enters the observation section at t_2. The flow then drops by a certain amount. From then on, (the mean value of) the flow decays exponentially until the driver has emptied. Thus, the shock wave exhibits a constant overpressure for a certain period of time, and then the pressure drops exponentially (Figure 15 bottom). The duration of the shock wave depends on the volume of the driver (for a constant-area shock tube, as is illustrated as an example, it depends on the length of the driver).

Several characteristic distances have to be considered when determining the location of the test section:

- Depending on the opening time of the membrane, a certain travelling distance is needed for the primarily-formed compression wave to steepen into a shock. Five tube-diameters are considered to be the absolute minimum.
- Since the initial rarefaction wave will eventually catch up with the shock front, there is a point downstream to which there is no longer a constant flow. If the constant-flow conditions are to be utilised, the test section has to be placed upstream to this point.
- The simulator downstream from the test section must be long enough to delay the waves which return from the end of the driven section for an adequate period of time so that they do not distort the measurements. In the example in Figure 16 the rarefaction wave from the opened end accelerates the pressure decay at $t=t_3$.

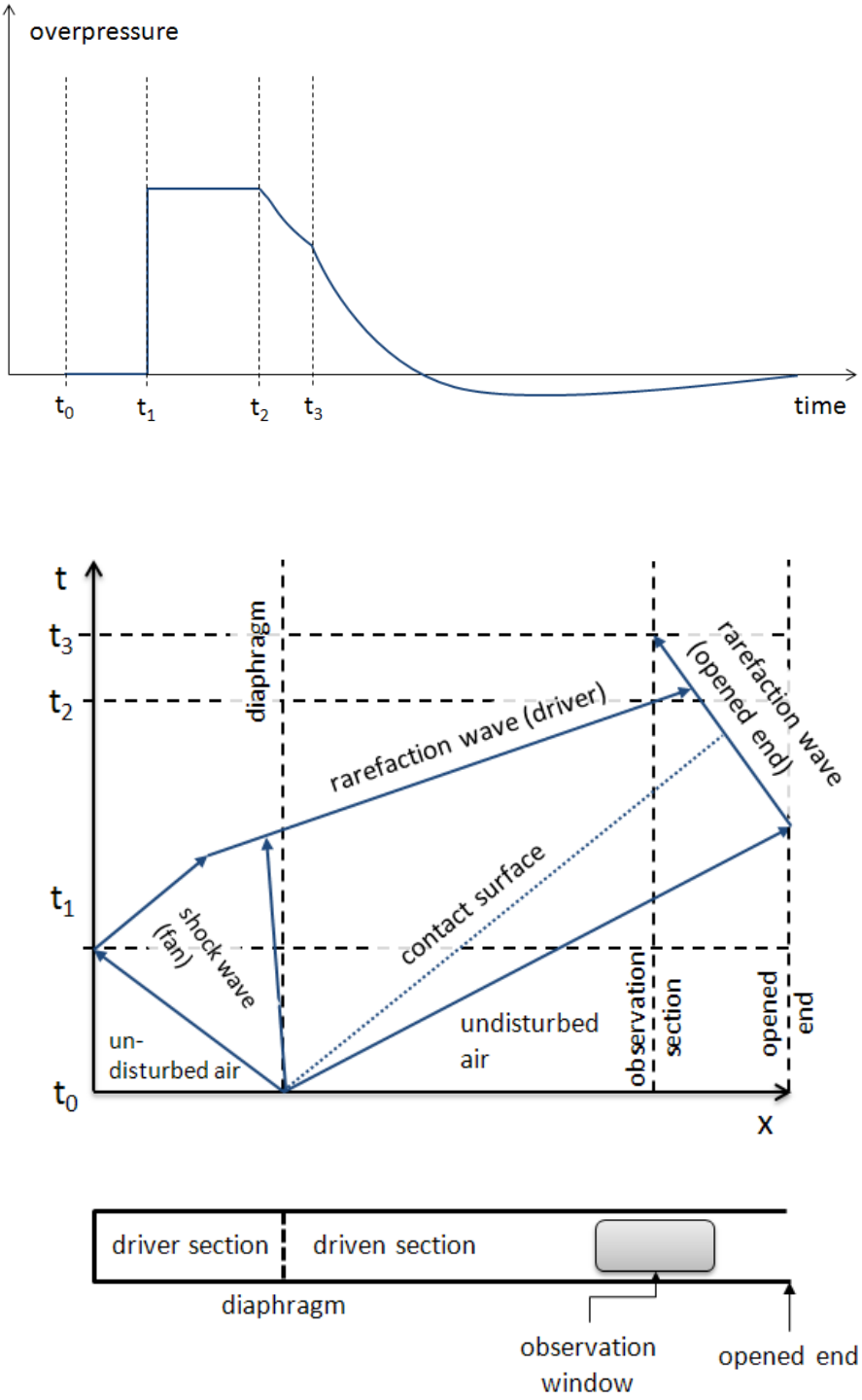

Figure 16: Example of the effect of the rarefaction wave from the open end of the shock tube

In order to use these effects to find the optimum pressure load setting, various kinds of constructions have been developed.

One of them is a rarefaction wave eliminator (RWE). Distorting waves, reflected from the tube end, can be almost completely avoided by equipping the downstream end of the shock tube with a

properly designed RWE. This is a device which partially covers the open tube end. It produces reflected shock waves from the flow blockage part and rarefaction waves from the open part to the atmosphere. With a proper selection of open-to-closed ratio these different types of waves will cancel each other out. This device will also help to smooth the transition from overpressure to negative pressure and to control the maximum negative pressure value.

Another possibility is a passive, built-in RWA which minimises the pressure decrease caused by rarefaction waves. An example is shown in Figure 17. To achieve a decaying loading function instead of a step-like one, an air vent with suitable discharge rate is also applied.

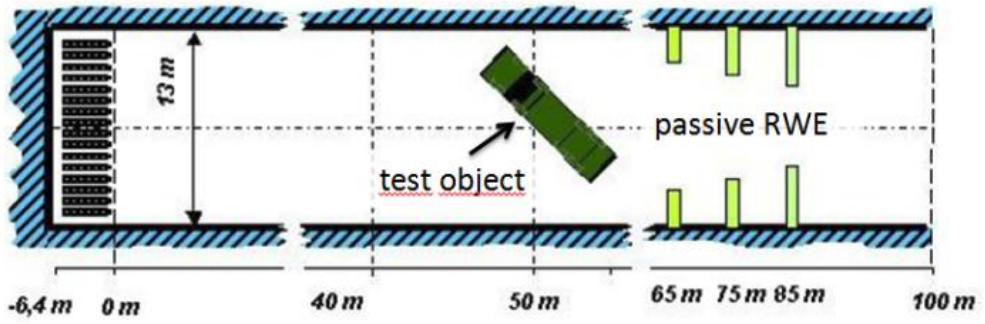

Figure 17: Passive-type RWE

In Figure 18 several possibilities for reducing the reflection phenomenon of blast waves in shock tubes are shown. Due to the closed-end section wall, and if the tested element has not failed, in some shock tubes the blast wave cannot leave the tube, thus leading to reflections. Through an exhaust, integrated at the beginning of the expansion part, a large portion of the blast wave can be led out of the tube. Secondary loading pulses acting on the test-element can be reduced strongly by this methodology.

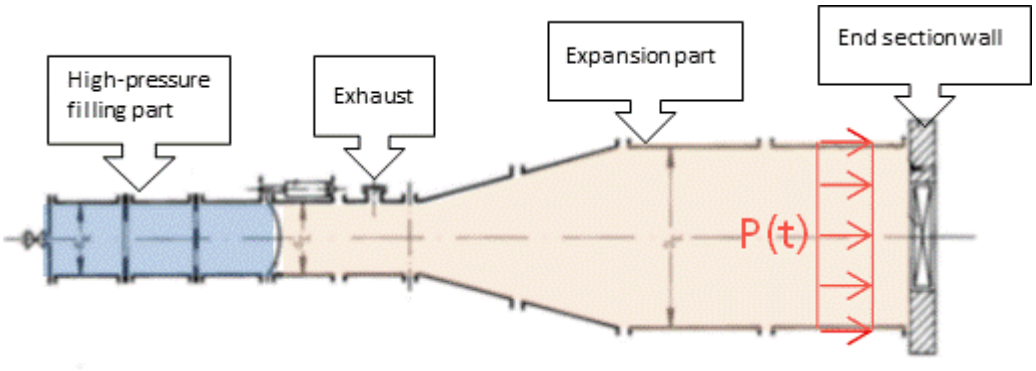

Figure 18: Schematic experimental set-up of a shock tube with a closed-end section and exhaust to release the blast wave

In addition, the discharge flow of the driver can be controlled to influence the pressure-time history of a shock wave in a shock tube. This can be achieved by controllable valves instead of membranes,

or by applying multiple driver tubes with different lengths or different filling pressures (Figure 19). This solution is especially useful for large pressurised air-driven blast simulators because of the large volume of air needed.

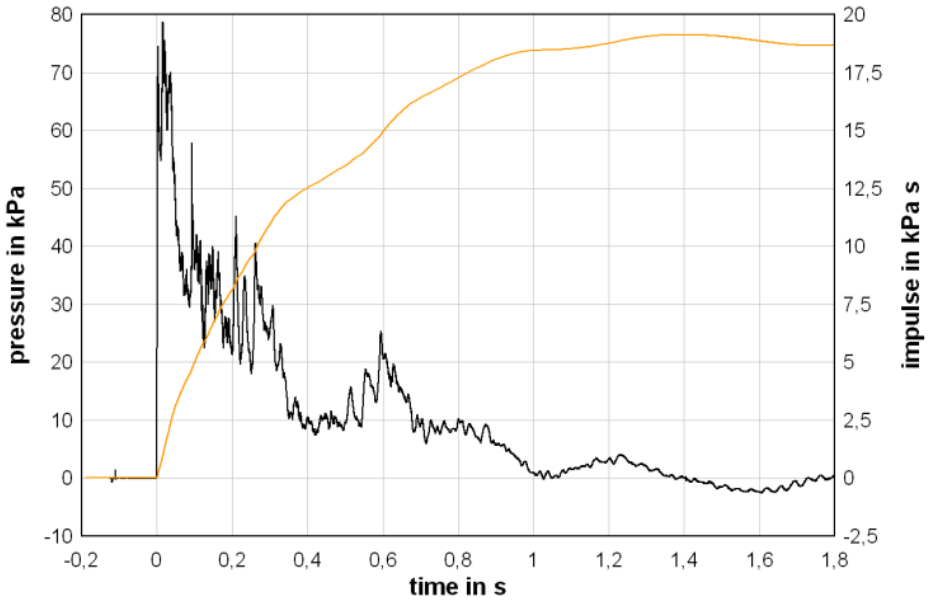

Figure 19: Realistic measurement in a shock tube with multiple driver tubes

2.3 The impact of shock waves on a specimen

2.3.1 High explosives

The effect of range on the shock front — The shock wave expands spherically from the site of the explosion and, depending on the range and relative size of the test sample, this may result in the load varying across the test sample. However this represents the real situation. As the range increases it may be reasonable to assume that the spherical wave front has become a plane wave front.

The effect of the charge being above the ground — If the explosion is above the ground the initial shock wave will impinge on the ground surface before reaching the test cubicle and continue to propagate along the surface. This reflected wave catches up and interacts with and reinforces the direct (incident) wave, the combined waves form the Mach front. Some variation in pressure over the height of the Mach front occurs but this is generally neglected and it is assumed to be uniform over its full height. This is to be used as the peak incident pressure on the Kingery-Bulmash (Kingery et al., 1984) curves for Air Burst explosions. The height of the Mach front increases as it travels away from the explosion and the top of the Mach front is known as the triple point (Figure 20). Above the triple point the pressure is more complex, as it is the sum of the incident and the ground reflected pressures.

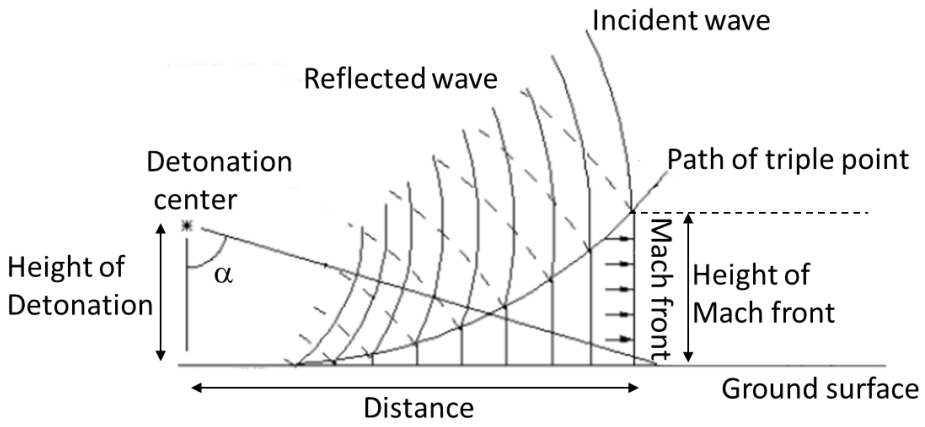

Figure 20: Development of Mach front and track of Triple Point according to UFC (UFC, 2008)

Clearing effects — For an infinite reflecting surface the duration of the positive pressure phase is t_d and the front face will experience an immediate rise to the peak reflected pressure. Due to the limited size of a test cubicle the blast wave is able to clear around the cubicle.
The reflected pressure will be relieved by a clearing wave with a clearing time, t_C, represented by:

$$t_c = \frac{4S}{C_r(1+R)} \tag{2.3-1}$$

where,

H is the height of the cubicle
W is the width of the cubicle
S is the clearing distance, the smaller of H or W/2
G the larger of H or W/2
R is S/G
C_r is the sound velocity in the reflected region

Once clearing has started the instantaneous pressure acting on the front face will be P, where:

$$P = P_S + C_D\, q \tag{2.3-2}$$

where,
P_S is the incident pressure (measured using a free field side-on gauge)
C_D is the drag coefficient for the cubicle, usually taken as unity
q is the dynamic pressure (the additional pressure caused by the blast wind)

The pressure-time history can be represented by an idealised bi-triangular trace (Figure 21) and the cleared impulse, $\mathbf{I_c}$, acting on the front face of the cubicle can be calculated, using values derived from the Kingery-Bulmash (Kingery, et al., 1984) curves for Air Burst explosions, as:

$$I_c = (P_{so} + C_D q_o)\, t_d / 2 + (P_{ro} - (P_{so} + C_D q_o))\, t_c / 2 \qquad (2.3\text{-}3)$$

where,

P_{so} is the peak incident pressure

P_{ro} is the peak reflected pressure

q_o is the peak dynamic pressure

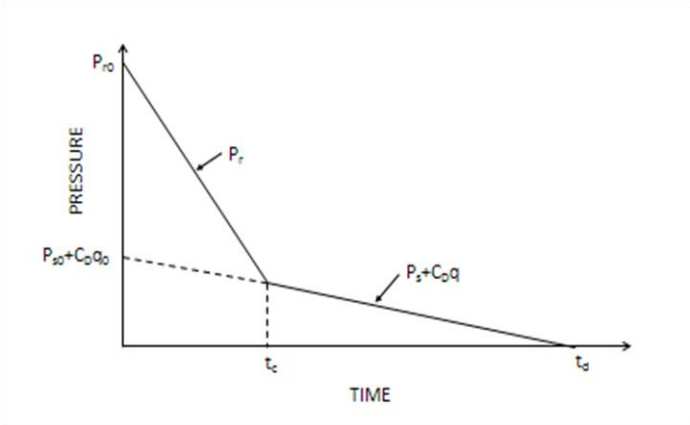

Figure 21: Idealised pressure-time history with clearing

Test conditions — When using an open test range it is necessary to understand the properties of the materials in the test sample to ensure that the test temperature does not adversely affect the sample's behaviour. If this is likely, measures to control the temperature will be needed or the test may have to be delayed.

2.3.2 Shock tube

A main parameter of interest when selecting a suitable blast simulator is the area of the test section. When a façade structure has to be tested, there are two ways of erecting it in a simulator. When the specimen is almost as large as the simulator it should be possible to install it at the end of the shock tube or in the test section tightened to the walls of the shock tube with a surrounding lining. In this case the specimen closes the end of the shock tube.

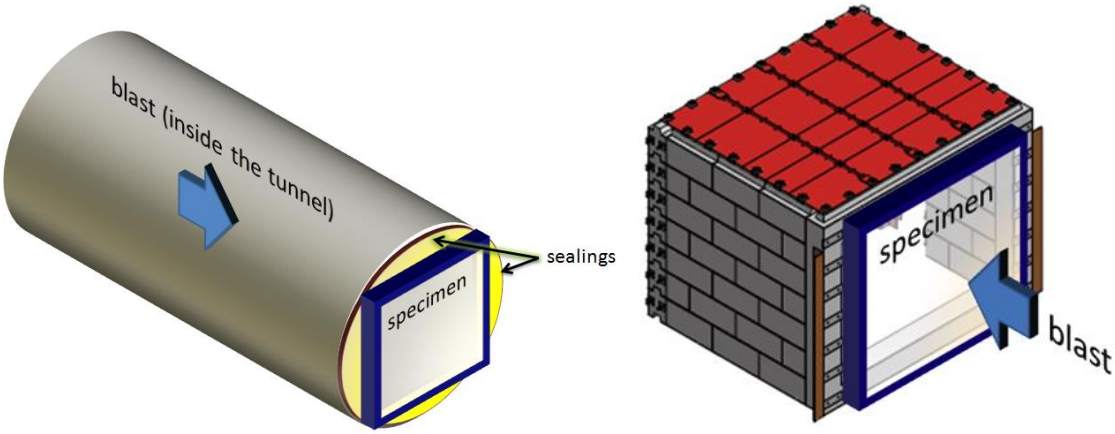

Figure 22: Specimen mounted on the shock tube end or on a reinforced structure

When the simulator is clearly bigger than the test object and the shock tube needs an open end, the diameter of the test section must be large enough to ensure that the blast-induced load on the test object is identical to that encountered in a free-field situation. If a façade element has to be tested it has to be mounted on a hardened structure that creates a room behind the specimen. This is necessary to prevent the shock wave from impacting the specimen on the rear, and in case of a glazing element, it is additionally needed for analysing glazing fragments. A common practice is to mount the façade element supported by a steel testing frame as a discrete wall on a room-like reinforced concrete structure (Figure 22).

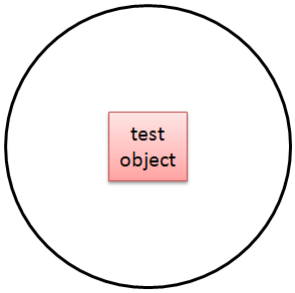

Figure 23: Visualisation of the blockage ratio of approximately 15 %

The influence of the limited size of the test section on the loading of the target is called the blockage effect. Any test object will present an obstruction to the flow in the test section. The extent to which the flow becomes disturbed by the test object depends on the blockage ratio. This is the ratio of the object's surface area facing the shock wave to the cross-sectional area of the test section, as indicated in Figure 23.

Two types of distortions of the loading functions may occur:

- Firstly, during the diffraction-loading phase, waves which originate from the interaction of the shock wave with the target may be reflected by the walls of the simulator. This causes local disturbances of the pressure distribution around the target.
- Secondly, a more severe distortion may occur during the drag phase. Due to the flow obstruction by the target, the flow velocity in the constricted region will be increased, thus enhancing the drag loading. Consequently, a target might be overturned at significantly lower overpressures than under free-field conditions.

The allowable blockage ratio may be calculated by using the 15 % rule often applied in such cases. It should be noted, however, that the allowable blockage ratio is closely interconnected with the target response time. A target which can be damaged during the diffraction loading phase may well block the simulator by 30 % or even more without showing a significant difference in its response compared to a target loaded under free-field conditions. On the other hand, if the displacement of a target is to be tested, good results are likely to be achieved only if the blockage ratio is 5 % or less.

For certification purposes, usually a load scenario is required that includes figures regarding reflection pressure and impulse and positive phase duration. As far as the test is concerned, this

means that the desired numbers must be exceeded at the location of the specimen. Note that the pressure on the surface of the specimen can vary substantially, depending on the load parameters, shock tube, flatness of the shock front, set-up and specimen geometry (Figure 24). However, there is usually no requirement regarding the exact spot for pressure measurement. Additionally, in most cases there is no definition of whether the specified value is to be exceeded by the average pressure over the surface or by the peak pressure.

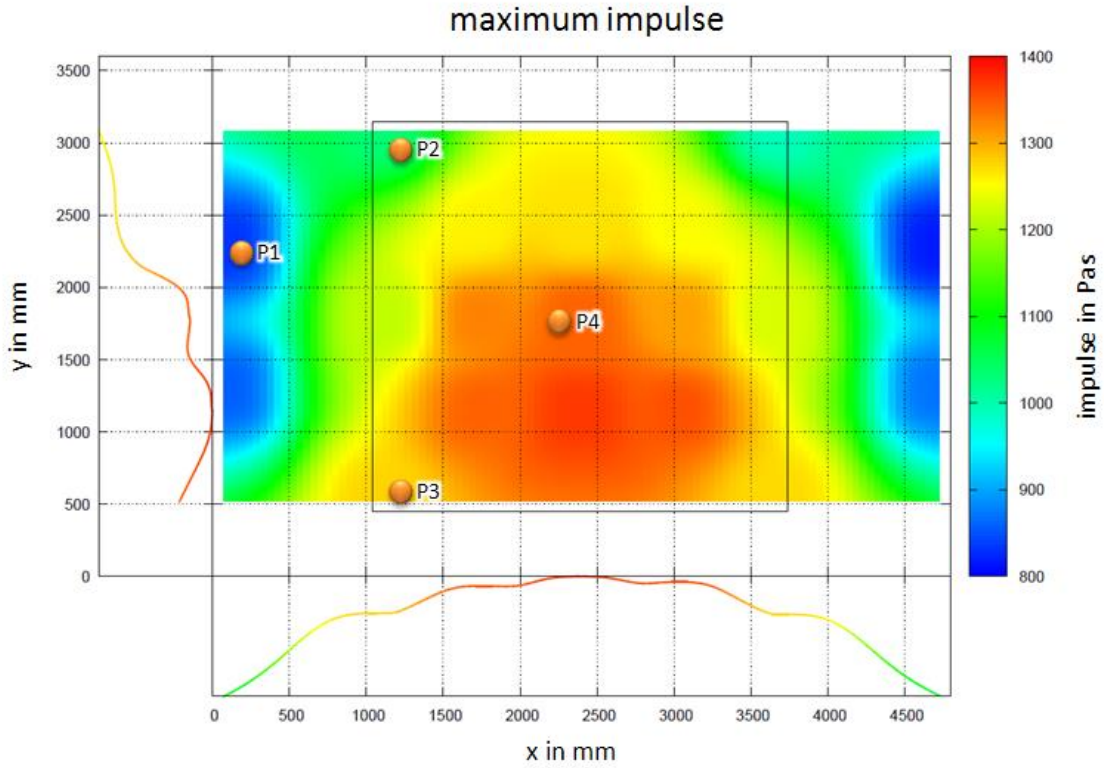

Figure 24: Pressure distribution on a test surface

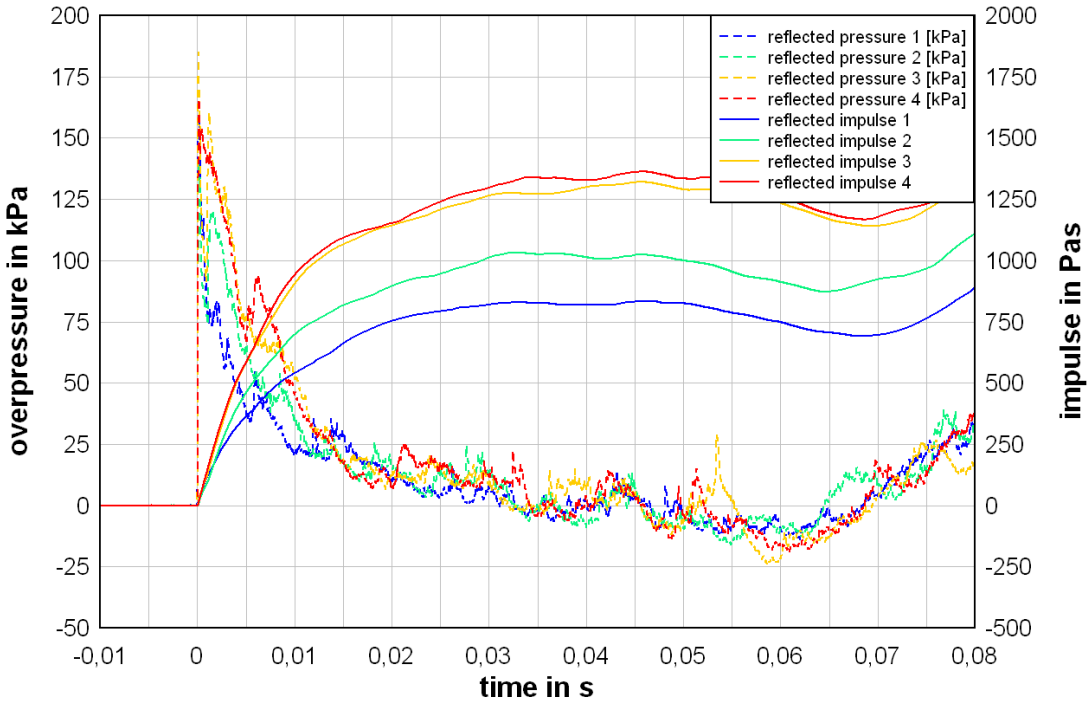

Figure 25: Impulse-time histories referring to the figure above

If the test object is attached to the end of the shock tube, the pressure and impulse gradients are of less significance than if placed inside the tube. Pressure waves that run into corners are compressed for a longer time than those that impact flat surfaces like the middle of the specimen, while those that hit the object near its free edges have the shortest duration.
This is why the size of the entire test set-up compared to the specimen itself is of high significance: in the event that the specimen is attached to the end of the tube, the set-up is comparable to an infinitely large facade. This ensures that the loads during the tests exceed the loads in real constructions. However, if, due to the size of the specimen, it is necessary to conduct tests in a large blast simulator and to attach the specimen to a rigid structure, the size of the area around it becomes critical.

If long pressure duration is desired, the eigenfrequency (fundamental period) of the specimen is critical. If the reaction time of the specimen is shorter than the positive pressure phase, one must ensure that the pressure doesn't decrease too much before the maximum deformation occurs, because otherwise the specimen could be loaded insufficiently, even under the correct pressure.

2.4 List of references

Riedel, W. 2004. Beton unter dynamischen Lasten Meso- und Makromechanische Modelle und ihre Parameter. Forschungsergebnisse aus der Kurzzeitdynamik, Heft 4.

CEN, 2001, EN 13123-1: Windows, Doors and Shutters — Explosion Resistance — Requirements and classification — Part 1: Shock Tube.

CEN, 2001, EN 13123-2: Windows, Doors and Shutters — Explosion Resistance — Requirements and classification — Part 2: Range test.

CEN, 2001, EN 13124-2: Windows, Doors and Shutters — Explosion Resistance — Test Method — Part 1: Shock Tube.

CEN, 2001, EN 13124-2: Windows, Doors and Shutters — Explosion Resistance — Test Method — Part 2: Range test.

CEN, 2000, EN 13541: Glass in building — Security glazing — Testing and classification of resistance against explosion pressure.

Gebbeken, N., Döge, N. and Hübner, M. 2012. Vom Explosionsszenario zur Bemessungslast. 5. Workshop 'BAU-PROTECT' Sicherheit der baulichen Infrastruktur vor außergewöhnlichen Einwirkungen.

ISO 16934: 2007 Glass in Building — Explosion-resistant Security Glazing — Test and Classification by Shock-tube Loading.

ISO 16933:2007/Cor1:2008 Glass in building — Explosion-resistant security glazing — Test and classification for arena air-blast loading.

Kingery C.N, Bulmash G, 1984. Technical report ARBRL-TR-02555: Air blast parameters from TNT spherical air burst and hemispherical burst. AD-B082 713, U.S. Army Ballistic Research Laboratory, Aberdeen Proving Ground, MD.

Kinney, G.F. and Graham, K.J. 1985. Explosive Shocks in Air. Second Edition, Springer Berlin.

Riedel, W., et al. 2010. Engineering and Numerical Tools for Explosion Protection of Reinforced Concrete. International Journal of Protective Structures..

Sauer, M., Klommfass, A. and Thoma, K. 2005, Interaktion von Detonationswellen und Gebäuden. Seminar Interaktionsprobleme im Ingenieurbau. Technische Universität Dresden.

Unified Facilities Criteria 2008, UFC 3-340-02 Structures to Resist the Effects of Accidental Explosions, U.S. Army Corps of Engineers, Naval Facilities Engineering Command, Air Force Civil Engineer Support Agency.

3 Measurements

3.1 Overview of instrumentation

The instrumentation at the test set-up and the supporting structure should allow the complete documentation of all the relevant data necessary for an appropriate evaluation of the test results in terms of correct loading and damage analysis. This comprises not only the relevant data from the resulting shock wave and shock-wave propagation (e.g. side-on pressure, peak overpressure on — or if not possible near — the sample, reflected pressure, interior air blast pressure within the supporting structure, etc.), but also climate data.

The air-blast pressure transducers should be capable of defining the anticipated air-blast pressure-time history within the linear range of the transducer and shall be calibrated prior to the blast test. Special pressure transducers and high-sampling rate (>100 kHz) acquisition systems are needed for highly dynamic applications. Furthermore, a high-speed camera should record the response of the test specimen in order to allow an optical assessment of the failure process of the test specimen.

Table 3 below lists the options for measurements in both types of test set-ups, explosives and shock-tube tests. For certification, the minimum measurement plan should contain:

1) Registration of the pre-test situation, e.g. by taking pictures;
2) Registration of the climate conditions (air temperature, humidity and pressure, as well as specimen temperature) within 30 min prior to the test;
3) Measurement of the shock load;
4) Registration of the post-test situation, e.g. by taking pictures.

Table 3: Measurement options

Objective	Measurement	Location and number	Obligatory for certification or special
Specimen	Pre-test pictures	At the relevant positions	Obligatory
Climate	Temperature	1	Obligatory
	Humidity	1	Obligatory
Load	Reflected pressure in the shock-tube test	At least 1 gauge adjacent to the test specimen. Duplication is recommended.	Obligatory The regulations state an obligatory total number of 2 pressure gauges without a specification if both are to measure the reflected pressure.
	Reflected pressure in the field test	2-3 gauges on concrete blocks at the same distance from the charge as the test specimen, or on the test cubicle adjacent to the test specimen.	Not obligatory following DIN EN 13124 GSA: Two air-blast transducers on each reaction structure.
	Incident pressure in the shock-tube test	1 gauge at a short distance (e.g. 1 m) in front of the test specimen.	Obligatory if only 1 gauge measures the reflected pressure. Helpful in the event of malfunctioning of reflected pressure sensor. Used for triggering.
	Incident pressure in the field test	2 gauges in the free field at the same distance as the test specimen.	Obligatory to ensure full detonation. Helpful for extrapolation with CFD.
Response	Post-test pictures		Obligatory
	Witness panels / debris catcher	3 m behind the test specimen.	Obligatory for tests with hazard classification.
	Normal video	Face-on or side view.	Alternative method to register both pre-, post and test situations. Helpful for registering post-test creep failure (relevant for pvb and polycarbonate glazing).
	High-speed video	Face-on view	Not obligatory, but an alternative method to register both pre-, post and test situations.
		Side view	Not obligatory, but an alternative method to register both pre-, post and test situations (hazard).
	Crack formation with breaking circuits		Special
	Displacement	On the test specimen, and support; tailor made.	Special
	Strains	On the test specimen; tailor made.	Special
	Velocity	On the test specimen; tailor made.	Special
	Acceleration	On the test specimen: tailor made.	Special
	3D measuring technique		Special
Hazard	Pressure	Leak pressure	Special

3.2 Detailed issues

3.2.1 Pressure measurements

Regarding the pressure measurements for shock-tube tests, only the reflected pressure is sufficient. However the incident pressure is also useful. A single measurement is sufficient, as there is (should be) a uniform shock wave through the cross-section of the shock tube. Minimising the probability of no measurement result due to gauge failure could be a reason for duplicating the pressure measurement.

In field tests, multiple pressure measurements are needed. Most of the standards prescribe a minimum of two air-blast transducers used on each test reaction structure to measure the pressure-time waveform acting on the exterior surface of the test. It is recommended to use pressure transducers which verify the full detonation of the high explosive. In practice three gauges are preferred in order to be able to understand the possible differences.

Pressure gauges are to be placed adjacent to the test specimens or on separate concrete blocks at the same distance in order to avoid gauges on the test specimen itself, as in that case they would influence the response.

3.2.2 Assessment of hazard

In this case, hazard classification is an issue in the test; also the hazard should be registered by using witness panels, or debris catchers behind the test specimen within the enclosed reaction structure. The witness panel should be made of expanded polystyrene or expanded foam and should be covered with an aluminium sheet or paper to record penetrations and/or perforations. The different standards prescribe slightly different distances for the witness plates, i.e. 3 m (ISO) 10 ft (3048 mm) (General Service Administration GSA, 2003) from the interior face of the window glazing.

The evaluation of the performance of glazing and windows systems against blast loads is based on the post-test location of fragments and debris relative to the original (pre-test) location of the window and can be rated according to the performance criteria. In the following, the classification defined by GSA-TS01-2003 (General Service Administration GSA, 2003) is presented as an example. The assessment criteria in the ISO standard are similar.

A schematic illustration of the GSA scheme used for classifying the performance conditions for window systems' responses is given in Figure 26. This scheme also includes the evaluation of a witness panel mounted at the inner rear side of the supporting structure.

The classification of the tested window systems results from the defined performance conditions as indicated in Table 4.

Table 4: Hazard rating criteria according to ISO 16933 (ISO).

Definition	Hazard-rating description	Hazard rating
The glazing is observed not to fracture and there is no visible damage to the glazing system	No break	**A**
The glazing is observed 10 fracture but the inner, rear face leaf is fully retained in the facility test frame or glazing system frame with no breach and no material is lost from the interior surface. Outer leaves from the attack face may be sacrificed and may fall or be projected out.	No hazard	**B**
The glazing is observed 10 fracture. Outer leaves from the attack face may be sacrificed and may fall or be projected out. The inner, rear face leaf shall be substantially retained, with the total length of tears plus the total length of pullout from the edge of the frame less than 50 % of the glazing sight perimeter. Also, there are no more than three rateable perforations or Indents anywhere in the witness panel and any fragments on the floor between 1 m and 3 m from the interior face of the specimen have a sum total united dimension of 250 mm or less. Glazing dust and slivers are not accounted for in the hazard rating. If by design intent there is more than 50 % pullout but the glazing remains firmly anchored by purpose-designed fittings, a rating of C (minimal hazard) may be awarded, provided that the other fragment limitations are mal. The survival condition and anchoring provisions shall be described in the test report.	Minimal hazard	**C**
The glazing Is observed to fracture and significant parts are located no further than 1 m behind the original location of the rear face. Parts be projected any distance from the attack face towards the blast source. Also, there are no more than three rateable perforations of indents anywhere in the witness panel, and any fragments on the floor between 1 m and 3 m from the interior face of the specimen have a sum total united dimension of 250 mm or less. Glazing dust and slivers are not accounted for in the rating.	Very low hazard	**D**
The glazing is observed to fracture, and glazing fragments or the whole of the glazing fall between 1 m and 3 m behind the interior face of the specimen and not more than 0,5 m above the floor at the vertical witness panel. Also, there are 10 or fewer rateable perforations in the area of the vertical witness panel higher than 0,5 m above the floor and none of the perforations penetrate more than 12 mm.	Low hazard	**E**
Glazing is observed to fracture and there are more than 10 rateable perforations in the area of the vertical witness panel higher than 0,5 m above the floor, or there are one or more perforations in the same witness panel area with fragment penetration more than 12 mm.	High hazard	**F**

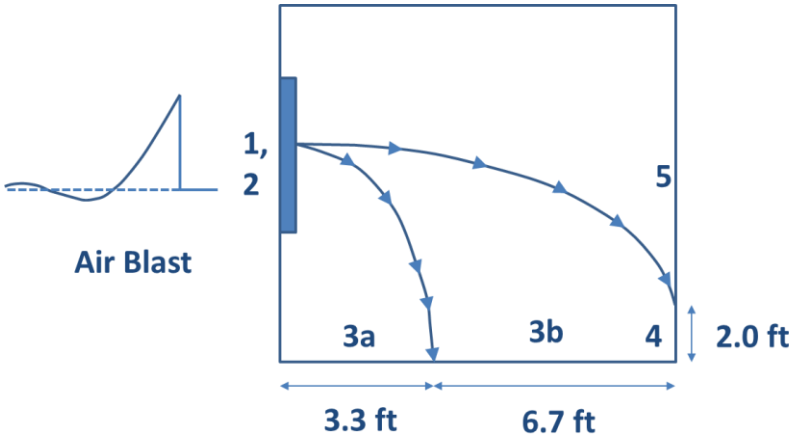

Figure 26: GSA/ISC performance conditions for window systems' responses according to GSA-TS01-2003 (General Service Administration GSA, 2003).

3.2.3 Post-test pictures

Furthermore, the location of any fragments/debris in the supporting structure, the test frame(s), and the test site/apparatus is photographically documented after the test and reported. The fragments/debris are documented as follows:

- Entire view of the test field from the side that is exposed to the blast load (front side);
- Entire view of the test field from the side that is not exposed to the blast load (rear side);
- Overall view of the samples from the front side;
- Detailed view of the samples from the front side;
- Overall view of the samples from the rear side;
- Overall view of the fragments/debris from the rear side (if applicable);
- Detailed view of the fragments/debris from the rear side (if applicable);

3.2.4 Videos

Videos are not obligatory, but are an alternative for registering the test specimen at different stages. As videos not only provide insight in the test specimen before and after the test but also during the test, they provide extra information, which is also very useful. Furthermore, videos are more illustrative in showing the classification of the tested product. In addition, high-speed videos offer the opportunity to follow the response step-by-step.

3.2.5 Special measurements

The other measurements listed are not necessary to show whether a product does meet the requirements, i.e. does it resist or fail the test load? These measurements are needed if one wants to extrapolate the test results by using calculation tools, or to verify calculation models. It is not

possible to describe a fixed measurement set-up for these gauges, since this will always be tailor-made, based on the test specimen and objective. However, some points can be made:

- It is recommended to have no gauges on the specimen, as they influence the response. Contactless gauges (e.g. laser gauges for displacement) are preferred. However, this is not always possible (e.g. accelerometers and strain gauges). It therefore always needs to be evaluated whether the response is not significantly influenced by the gauges.
- As the shock tube does not provide a rigid supporting structure for the test specimen, the response of the shock tube also needs to be registered, in order to extract the net response of the test specimen.
- The measurement of strains usually makes sense only if the strain is measured on two faces, i.e. the loaded face and rear face.
- The 3D-measuring technique is a relatively new technique. By applying markers on the surface of the test specimen and using two cameras, high-speed videos can provide response information about the product at any point in time thanks to supporting analysis techniques.

3.3 List of references

CEN, 2001. EN 13123-1: Windows, Doors and Shutters — Explosion Resistance — Requirements and classification — Part 1: Shock Tube.

CEN, 2001. EN 13123-2: Windows, Doors and Shutters — Explosion Resistance — Requirements and classification — Part 2: Range test.

CEN, 2001. EN 13124-2: Windows, Doors and Shutters — Explosion Resistance — Test Method — Part 1: Shock Tube.

CEN, 2001. EN 13124-2: Windows, Doors and Shutters — Explosion Resistance — Test Method — Part 2: Range test.

ISO 16934: 2007 Glass in Building — Explosion-resistant Security Glazing — Test and Classification by Shock-tube Loading.

ISO 16933:2007/Cor1:2008 Glass in building — Explosion-resistant security glazing — Test and classification for arena air-blast loading.

GSA -US General Services Administration 2003. Standard Test Method for Glazing and Window Systems Subject to Dynamic Overpressure Loadings, GSA-TS01-2003.

4 Interpretation of pressure-time histories

4.1 Determination of shock-wave parameters

Pressure-time readings need to be smoothed and analysed with filters in order to eliminate sharp spikes arising from recording and instrumentation irregularities. Firstly, the loading characteristics can be extracted from the measured signals, i.e. the peak pressure p_{peak}, the impulse and the positive phase duration (e.g. Figure 27).

The peak pressure should not be read from the real recorded signal, but from the Friedlander curve (CEN, 2001; Kinney et al., 1985) that best fits the pressure record. The same curve should be used to determine the positive phase duration.

The impulse is determined by integrating the pressure-time signal and reading the maximum value of the integrated signal. This maximum value occurs at $t=t_{pos}$; the positive phase duration. Note that noise in the recorded signal can give rise to a non-zero impulse at the start of the shock load. If that is the case, the value at t_0 should be subtracted from the value at $t=t_{pos}$.

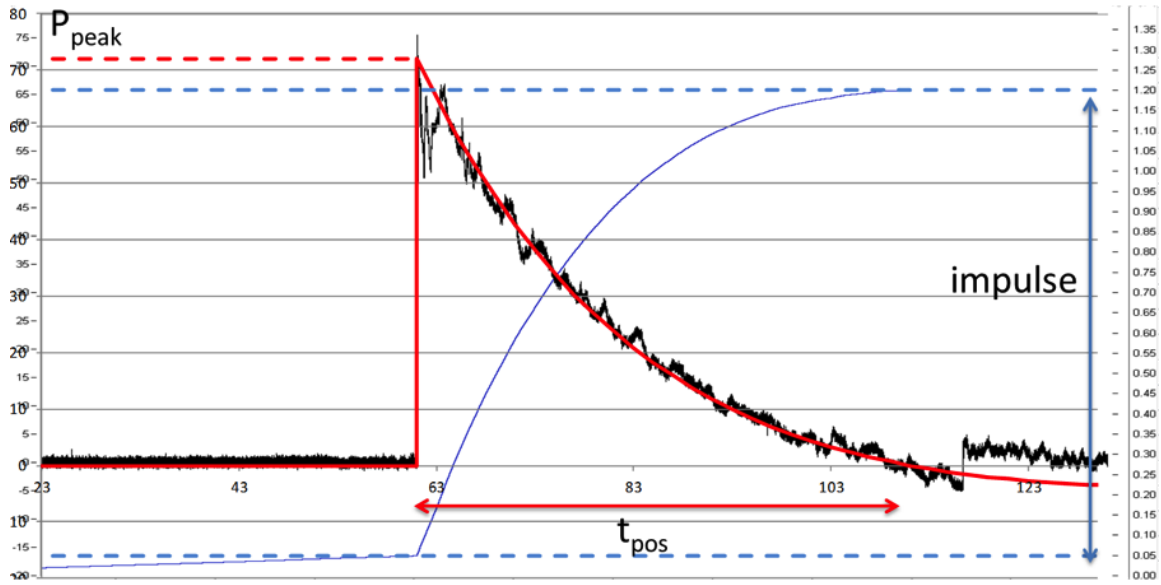

Figure 27 Example of a pressure-time signal, main characteristics and fit with Friedlander curve

A test qualifies the blast resistance of a window or glazing for a real scenario only if the loading in the test is equal to or higher than that of the defined scenario. This means that both the peak pressure and the impulse of the reflected pressure must meet this condition. The positive phase duration should not deviate too much from the scenario required. In case of large deviations a blast expert should judge the qualification.

If the scenario conditions cannot be met with the shock tube or the arena test, it does not mean that the appropriateness of the window cannot be determined. However, the test set-up needs further tailor-made design with additional measurements, to be used for results extrapolation using calculation methods.

4.2 Interpretation of measurements in high explosives testing

The pressure-time waveform generated by the explosive charge is measured at different locations in order to characterise the resulting shock wave and to determine the maximum pressure acting on the test specimen. As the measured pressure-time waveform depends on the location of the measuring point, the data recorded by the pressure transducers mounted on the exterior wall of the supporting structure do not represent the actual blast load acting on the test specimen. This fact is caused because it is not possible to place air-blast pressure transducers on the surface of the tested sample.

If no extra instrumented measure blocks are used in the experiment, which are placed at the same distance to the detonation centre as the test specimen (Figure 28), the actual blast load acting on the test specimen can be calculated via the appropriate numerical calculations based on the recorded data of the pressure transducers located at defined points around the test specimen (Figure 28c). Using this approach, the clearing effect can also be considered. The numerical model is adjusted to the experimental data that are determined by the pressure transducers mounted on the exterior wall of the supporting structure. The initial model and the obtained results at time of 22.5 ms are depicted in Figure 28a and Figure 28b and are compared with experimental data in Figure 28d.

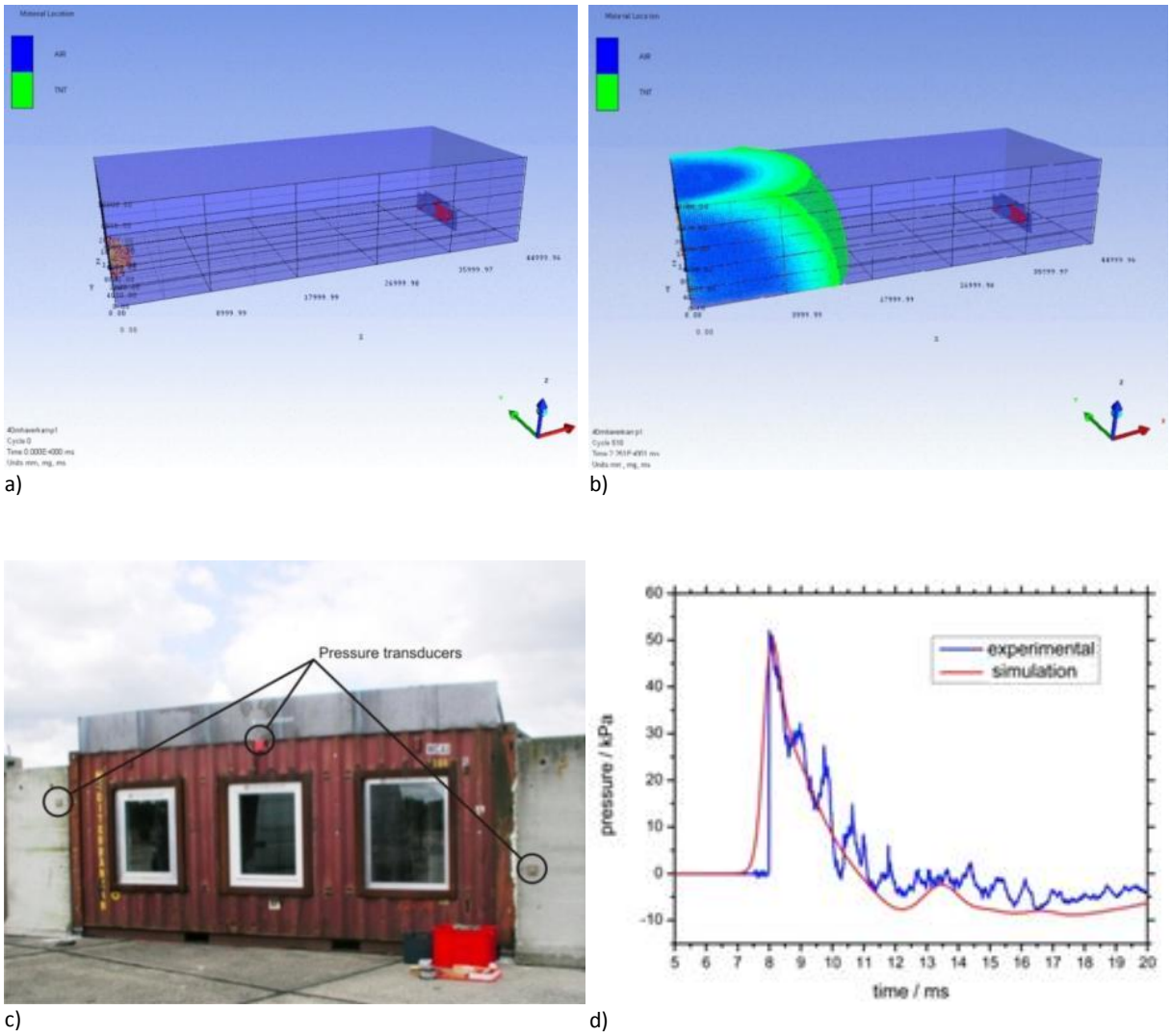

Figure 28: Numerical simulation of a blast test conducted according to GSA-TS01-2003: a) initial situation, time step 0.00 ms; b) propagating shock wave at time step 22.5 ms; c) experimental test set-up with location of the pressure transducers used for the numerical simulation; d) experimental vs. numerical results for one measuring point on the exterior wall

4.2.1 Recommendations

Recommendations on blast tests for glazing and window systems comprise both modifications on the set-up and additional measurements for assessing the fracture process. Modifications on the set-up are related to the supporting structure in order to obtain a more realistic scenario. Figure 29 shows modifications that can be made to the supporting structure. Here, the windows can be fixed according to a realistic situation in a building, which is either defined by masonry or, more rigidly, by a reinforced concrete wall. Furthermore, the area of the exterior wall that is directly subjected to the blast load can be enlarged in order to reduce the negative effects caused by clearing.

a) b)

Figure 29: Improved sample support to avoid blast-wave clearing

4.3 List of references

CEN, 2001. EN 13123-1: Windows, Doors and Shutters — Explosion Resistance — Requirements and classification — Part 1: Shock Tube.

Kinney, G.F. and Graham, K.J. 1985. Explosive Shocks in Air. Second Edition, Springer Berlin.

5 Review of numerical methods

Numerical methods have been developed in order to help engineers in understanding, analysing and predicting the physical phenomena occurring during different types of loading conditions. Numerical tools are of great importance, especially in the dynamic loading domain, because such quick events like blast loading are not easily understandable just by studying the damaged structure.

Two families of tools are usually employed to help engineers in order to analyse the blast effect on a structure:

- **Finite element tools,** which are time costly but allow a precise analysis of the phenomena of the interaction between the blast wave and the structure;
- **Engineering tools, which** enable quick parametric studies of structural response and damage but cannot give a precise description of the interaction between the blast wave and the analysed structure.

5.1 Implicit and explicit FEM

Numerical analysis can be advantageously used to predict the behaviour of glass undergoing blast-wave effects. These numerical simulations cannot replace experimental tests but they can be used in planning the tests, to predict experimental results and to carry out parametric studies by varying e.g. boundary conditions, the geometry of the structure, material properties and explosive data. Most FEM solvers are based on a representation of structural components by elements. Typically, elements can be 1D (a beam, for example), 2D (the shell, for example) or 3D (a brick, for example). Each corner (i.e. extremity) of an element is defined with a node. The assemblage of all elements represents the studied structure and eventually the environment of the structure (air, for example) and is called the meshed structure.

5.1.1 Numerical schemes

Implicit and explicit time integrations are the two main available methods used in finite element analysis. These methods have different time integration procedures. The most appropriate method is selected based on the nature of the problem to be solved.

The implicit method is unconditionally stable. This means that the accuracy of the solution is not dependent on the size of the time step. Large time increments can be used during the analysis and consequently the computation cost can be significantly reduced, particularly when the problem is linear. The only condition is that the time increment has to be sufficiently small to capture the time variation of the loading. In a linear analysis (linear material behaviour, no contact, small strain, etc.) the solution of the unknown variables (e.g. displacement components at the nodes) can be directly obtained from known variables established at the previous time step. There is no iterative process and the numerical procedure is very effective. For non-linear analysis with elastic and plastic materials, damage material models and contacts etc., an iterative procedure is required to get an accurate solution. In this case a convergence criterion is needed. For such non-linear problems, the computational cost increases significantly. In some configurations, when the time increment is too large, the convergence criterion cannot be satisfied and the time increment has to be reduced in order to obtain a convergence of the iterative procedure. For highly non-linear problems the convergence of the iterative procedure cannot be reached and the simulation stops. In these cases the computational cost becomes very high and selecting the explicit procedure can be advantageous.

The explicit method is conditionally stable and an iterative process is required to compute the solution at time $t + \Delta t$. The stability criterion is satisfied if, during the time increment Δt, the wave propagates a shorter distance than the smallest finite element size:

$$\Delta t \approx \frac{L_{\min}}{C_d} \tag{5.1-1}$$

where L_{min} is the smallest element dimension in the mesh and C_d is the dilatational wave speed.

This condition leads to very small time steps in comparison to the time increment of the implicit analysis. When the material behaviour is highly non-linear, with severe changes of the slope of the stress strain curve (e.g. concrete or any other brittle material), the explicit time integration scheme is recommended. This numerical procedure is also very effective to simulate shock-wave propagation phenomena and highly dynamic loading. It is also extremely adequate in simulating contact conditions where contact forces abruptly vary in space and in time. This method is recommended for predicting structural behaviour under explosion and impact effects.

When the material is highly deformed, the time increment during an explicit analysis can severely drop. This is a consequence of the stability criterion for the distorted finite elements that follow the material flow. For such elements the distance between opposite facets can be significantly reduced and consequently the time increment decreases drastically.

5.1.2 Solvers

The main two solvers are:

- Lagrangian solver;
- Eulerian solver.

The Lagrangian solver is the most commonly used in FEM analysis. The mesh represents the structure and its deformation. During blast loading, the structure may undergo large deformations and the calculation mesh may be highly deformed and thus cause the premature termination of the calculation.

To overcome this difficulty, the Euler formulation can be used instead of the standard Lagrange approach. In the Euler scheme the mesh (the grid) is fixed and the materials (solids, liquids and gases) flow through the grid. In this formulation, at each time increment, there are two phases:

- The first is the classical Lagrange phase where the solution to the problem is found considering that the mesh follows the material;
- The second phase is called the advection phase; in this phase, all quantities are computed (transported) through the fixed grid.

Eulerian analyses are effective for applications involving extreme deformation, up to and including fluid flow. In these applications, traditional Lagrangian elements would become highly distorted and

lose accuracy. Liquid sloshing, gas flow and most of the penetration problems can be handled effectively using an Eulerian analysis.

In the Euler scheme, the time integration procedure is mostly explicit. The disadvantage of the Euler approach is due to the possibility of having several materials in the same grid cell. This leads to more complicated numerical rules to estimate pressure, density and other variables when the grid contains several materials with diverse material models. The location and the motion of the contact interfaces between materials are not easy to follow. Moreover the transportation phase generates some additional errors in the numerical calculations.

In order to improve the quality of the numerical approach, many modern codes include coupled Euler-Lagrange analysis. In this case the space domain is separated into two parts. One part is devoted to the Lagrange analysis and the second part is kept for the Euler approach. This coupled approach is very useful in simulating, in a single run, the shock-wave propagation and the structure response. Eulerian-Lagrangian contacts allow the Eulerian materials to be combined with traditional non-linear Lagrangian analyses.

In a traditional Lagrangian analysis nodes are fixed within the material and elements deform as the material deforms. Lagrangian elements are always 100 % full of a single material so that the material boundary coincides with an element boundary. In a Eulerian analysis nodes are fixed in space and material flows through elements that do not deform the mesh. Eulerian elements may not always be 100 % full of material and many may be partially or completely void and a single Eulerian element can contain a mixture of multiple materials. The material boundary in an Eulerian mesh must be computed at each time increment. The Eulerian mesh is typically a simple rectangular grid of elements constructed to extend well beyond the Eulerian material boundaries, giving the material space to move and deform.

If no boundary conditions are specified, Eulerian material can flow freely into and out of the Eulerian domain through mesh boundaries. Typical boundary conditions for fluid or gas motion are sticky and sliding boundaries that restrict the flow in normal and/or tangential directions on the boundary.

Even solids can be modelled within the Eulerian framework, but the solution is not as accurate as the Lagrangian solution scheme. Liquids and gases can be modelled using equations of state; these include the ideal gas model utilised for air and the Jones-Wilkins-Lee (JWL) model utilised for the explosive material (Section 5.3.1). The analysis methodology is briefly outlined in this chapter and more details are available in (Dassault Systemes, 2012).

New methods appear in a high-speed/deformation simulation domain. One of them is the Smoothed Particle Hydrodynamics (SPH) method. SPH is a numerical method that is part of the larger family of mesh-free methods. For these methods it is not necessary to define nodes and elements as is normally done in a finite element analysis. It is necessary to define a collection of points representing a given body. In SPH these points are commonly referred to as particles or pseudo-particles. SPH is a fully Lagrangian modelling scheme permitting the discretisation of a prescribed set of continuum equations by interpolating the properties directly at a discrete set of points distributed over the solution domain without the need to define a spatial mesh. A Lagrangian solver coupled with the absence of a fixed mesh permits problem solving associated with fluid flow and structural interaction involving large deformations, failure and rupture of the structure.

5.1.3 Synthesis

Table 5 lists in alphabetical order some well-known software with their respective time-integration method. They are separated between commercial and organisation-developed. The name of the company/organisation which commercializes/develops the named software is noted in parentheses.

Table 5: Non-exhaustive FEM codes list with their time-integration methods and solver capabilities

Software	**Implicit Method**	**Explicit Method**	**Solver**			
			Lag	Eul	Eul/Lag	Other
Commercial software						
ABAQUS (Dassault Systems)	X	X	X	X	X	SPH
ANSYS (ANSYS)	X	X	X			
AUTODYN (ANSYS)		X	X	X	X	SPH
COMSOL (Comsol)	X	X				
IMPETUS (Impetus)		X	X			SPH
LS-DYNA (LSTC)	X	X	X	X	X	SPH
NASTRAN (MSC)	X	X	X			
PAM CRASH (ESI)	X	X	X			
RADIOSS (Altair Engineering)	X	X	X			
Organisation-developed software						
ASTER (EDF)	X		X			
CASTEM (CEA)	X	X	X			
EUROPLEXUS (CEA + JRC)		X	X	X	X	
OURANOS (CEA)	X	X	X	X	X	
SOPHIA (EMI)		X	X			

5.2 Coupled and decoupled approach

Structural analyses methods (based on FEM) for blast-wave loaded structures can be divided into two main groups:

- decoupled approach,
- coupled approach.

5.2.1 Decoupled approach

In the decoupled approach the pressure loading is calculated separately (using formulas -see Sections 5.3.1 and 5.3.2) from the structure response. The pressure transients are then given as loading functions to the structural analysis model. The individual pressure transient presents the pressure at the wall surface as a function of time. For example, the properties of the loading function are dependent on the scaled distance from the detonation point to the considered element of the structural-analysis model (as defined in Section 5.3.2). As the distance increases, the peak pressure value decreases and the duration of the pressure pulse increases. Also the arrival time depends on the scaled distance to the detonation point.

The decoupled approach is usually used:

- when the time response of the structure is longer than the pressure signal time (the eigenvalue of the structure usually determines this parameter);
- when the deformation of the structure doesn't significantly modify the pressure signal.

5.2.2 Coupled approach

The structural effects of explosions can be simulated using a Coupled Eulerian/Lagrangian finite element analysis technique (CEL).

By this approach, the real phenomenon of interaction between the air (shock wave) and the structure itself is analysed. The main difference from the decoupled approach is that the blast wave generates stress within the structure but the structure is also able to interact and modify the blast wave. This type of simulation is time costly and expensive in terms of computational resources because it needs to solve both Lagrangian and Eulerian equations at each time increment. This type of simulation is also used when successive structures are going to be loaded by the same blast wave (for example the corners of walls, walls behind windows, etc.).

5.3 Numerical models for structural response analysis under explosive loading

In order to assess the structural response under an explosive loading using numerical simulations two main issues have to be accomplished. First, the explosive loading has to be reproduced correctly within the simulation. Therefore specialised thermodynamic material descriptions are necessary. Second, an important issue of finite element analysis is the way to simulate non-linear material behaviour. Each solver uses standard models and also specific models dealing with the particular behaviour of materials. For example, in order to simulate the material behaviour of steel, it is

possible to use a classical elastic purely plastic model, but also an improved model such the Johnson-Cook model (details in Chapter 5.3.2). This chapter details some typical models used in most of software presented in 5.1.3.

5.3.1 Modelling detonation and shock waves

5.3.1.1 Equation of state models

The equation of the state material model is a hydrodynamic material model in which the material's volumetric strength is determined by an equation of state (EOS). These models determine the pressure stress as a function of the material density and the specific energy. The EOS models used in this work are the ideal gas model for free air, and the JWL equation of state for the high-explosive material.

5.3.1.2 Ideal gas model for air

The ideal gas model is used to model pressure-wave propagation in the free air surrounding the explosive material. The ideal gas equation of state reads

$$p = \rho R T \tag{5.3-1}$$

which can be written in an alternative form

$$p = (\gamma_\alpha - 1)\,\rho E \tag{5.3-2}$$

where γ_α is the adiabatic constant, E is the specific internal energy, p is the pressure, ρ is the material density, T is the current absolute temperature, and R is the specific gas constant defined for unit mass, i.e. in units $\mathrm{Jkg^{-1}K^{-1}}$.

5.3.1.3 JWL model for explosion products

The Jones-Wilkins-Lee (JWL) equation of state models the pressure generated in the explosion process as a function of the density of the explosion products. This model is implemented in a programmed burn manner where the detonation location and time of the explosion is specified as an initial condition. The detonation shock wave propagates from the initiation point with a specified detonation wave speed. After the material point has detonated, it starts expanding according to the equation of the state model. The JWL equation of state is

$$p = A\left(1-\frac{\omega\rho}{R_1\rho_0}\right)\exp\left(-R_1\frac{\rho_0}{\rho}\right) + B\left(1-\frac{\omega\rho}{R_2\rho_0}\right)\exp\left(-R_2\frac{\rho_0}{\rho}\right) + \omega\rho E_m \tag{5.3-3}$$

where p is the pressure, ρ is the density of the explosion products, ρ_0 is the initial density of the solid explosive and E_m is the specific internal energy of the explosive (internal energy per unit mass). A, B, R_1, R_2 and ω are the material model parameters that are determined experimentally for each explosive type. Values for these parameters can be taken from (Dobratz et al., 1985).

The pressure — volumetric expansion ($V/V_o=\rho_o/\rho$) behaviour of the JWL model, using typical TNT parameters, is shown in Figure 30, where the three contributing constituents are also drawn. The first term dominates in the initial phase of the explosion and in the final phase the model degenerates to the ideal gas model, described by the third term.

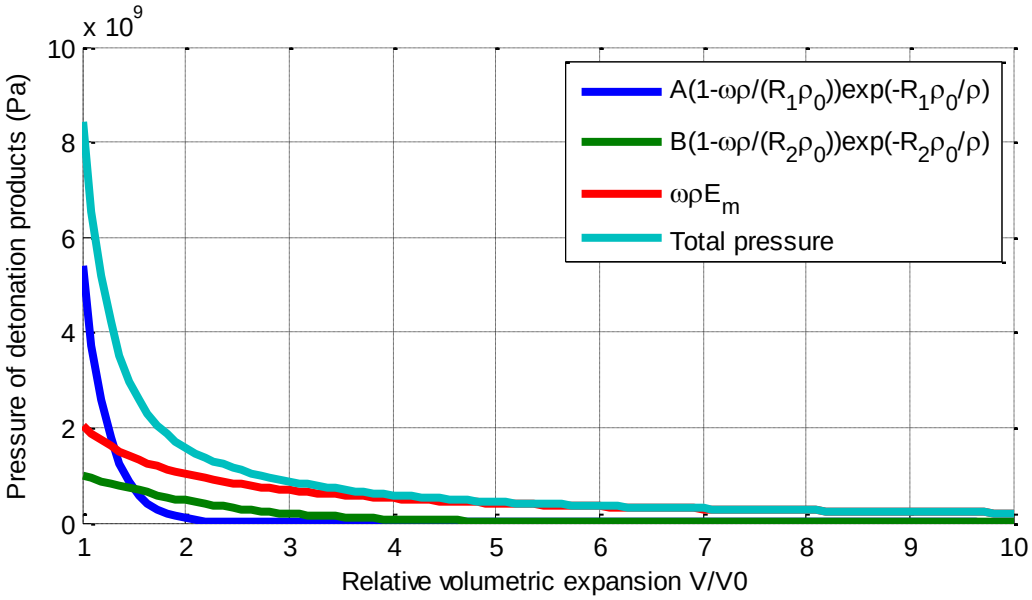

Figure 30: Pressure — volumetric expansion calculated with the JWL model using typical TNT parameters

5.3.2 Alternative calculation of analytical transient blast loads

Another model used to calculate the peak positive pressure is the modified Friedlander equation (Equation 5.3-4) which is a quasi-exponential approximation of the positive phase of the waveform accounting for the ambient pressure.

$$P_s\ t\ = P_{so}\left(1-\frac{t}{t_o}\right)e^{-(\alpha\frac{t}{t_o})} \qquad (5.3\text{-}4)$$

where t_o=duration of positive phase, α=constant, and P_{so}= peak overpressure. The peak overpressure, accounting for the ambient pressure p_o, can be calculated using the empirical formula

$$p_{so} = p_o \frac{808\left[1+\left(\frac{Z}{4.5}\right)^2\right]}{\sqrt{1+\left(\frac{Z}{0.048}\right)^2}\sqrt{1+\left(\frac{Z}{0.32}\right)^2}\sqrt{1+\left(\frac{Z}{1.35}\right)^2}} \tag{5.3-5}$$

where Z is the scaled distance defined by the actual distance divided by the cubic root of the charge weight, given in [m/kg$^{1/3}$], according to equation (2.1-2).

The positive specific impulse or impulse per unit area i_s [Pa·s] of the blast wave is the time integral over the positive phase of the side-on overpressure

$$i_s = \int_0^{t_0} P_s(t)\,dt \tag{5.3-6}$$

Inserting Friedlander's equation and performing the integration (CEN EN 13123-1) gives

$$i_s = P_{so}\, t_0 \left\{\frac{1}{\alpha} - \frac{1}{\alpha^2}\left(1-e^{-\alpha}\right)\right\} \tag{5.3-7}$$

The equation provides values for blast-wave impulse per unit area when the wave form parameter α is known. Inversely, knowing the blast impulse per unit area, the wave form parameter may be obtained from this equation.

Blast-wave parameters are usually plotted as functions of the Hopkinson scaled distance. These parameters are based on empirically defined equations and they should not be extrapolated beyond the ranges given in the literature (Kinney et al., 1985).

Shock arrival time to the impact location can be calculated according to the experimental data provided by (Kinney et al., 1985). This reference gives tabulated values of scaled shock wave arrival time $t_a/W^{1/3}$ as a function of the scaled distance Z for chemical and nuclear explosions.

When the shock impinges onto a wall surface, a new reflected shock is formed. The overpressure and temperature of the reflected shock may be significantly higher than those of the incident shock. When the shock wave is reflected from a large surface parallel with the wave front, the peak value of the reflected pressure P_{r0} [Pa] is

$$P_{r0} = 2P_{s0} + \frac{(\gamma_a+1)P_s^2}{(\gamma_a-1)P_{s0}+2\gamma_a p_a} \tag{5.3-8}$$

where P_{s0} is the peak value of the side-on overpressure, p_a is the atmospheric pressure and γ_a is the ratio of the specific heat capacities c_p/c_v of air. c_p is the specific heat capacity at constant pressure and c_v is the specific heat capacity at constant volume. Except for very high values of P_{s0}, air can be assumed to be a diatomic ideal gas with γ_a = 1.4.

When the angle of incidence β exceeds the limiting value β_m, the incident and reflected wave fronts merge forming the so-called Mach front. For values of M_x larger than about 1.2, the limiting value β_m can be estimated from the relation

$$\beta_m = 39° + \frac{1.75°}{M_x - 1} \tag{5.3-9}$$

where M_x is the Mach number. The relation between M_x and P_{s0} is

$$M_x = \sqrt{1 + \frac{6P_{s0}}{7p_a}} \tag{5.3-10}$$

where p_a is the atmospheric pressure (Kinney et al., 1985).

5.3.3 Material modelling

The simulation of air-blast loaded facades must consider all relevant structural parts. The first one is the glass itself which is described later in detail. Next is the modelling of the sealant and the frame of the window. Both of them constitute the boundary condition of the glass and should be modelled in detail since this condition has a strong influence on the glass failure behaviour. If the anchoring elements and the wall are too weak this must be included in the model, too.

If the window is part of a glass facade it is recommended to also model the facade system since this system is often more flexible than a stiff concrete wall and it absorbs a part of the blast energy by plastic deformations. These deformations of the facade can result in additional failure of the windows.

Double-glazing systems are more complicated to model since the gas in between the glass panes eventually transmits the loading to the second glass ply. After strong deformations both glass panes could also come into contact. Retrofitting systems with, for example anti-shatter film, can also be numerically modelled, but this will not be described here.

A crucial parameter in the numerical simulation of explosion effects is the definition and modelling of the material mechanical properties. The blast waves can cause significant structural deformation exceeding the linear domain and this implies that one has to deal with concepts such as plasticity, visco-plasticity, large strains, high strain-rate, failure and fragmentation etc. Features of the modelling of the main structural materials, such as glass, steel, aluminium and concrete, will be presented, and some elements of the more innovative materials, such as polymers, will also be included.

5.3.3.1 Glass

Glass is often the most fragile part of a structure and is therefore the most important part in order to protect critical infrastructure and its occupants. There are three different types of glass (Figure 31). They can be distinguished by their average failure strength which lies between 70 and 250 MPa. The

strength of one glass type shows strong variations due to micro-flaws. Dynamic glass strength still needs more investigations, but some experiments show a higher dynamic strength than the static one (Peroni et al., 2011).

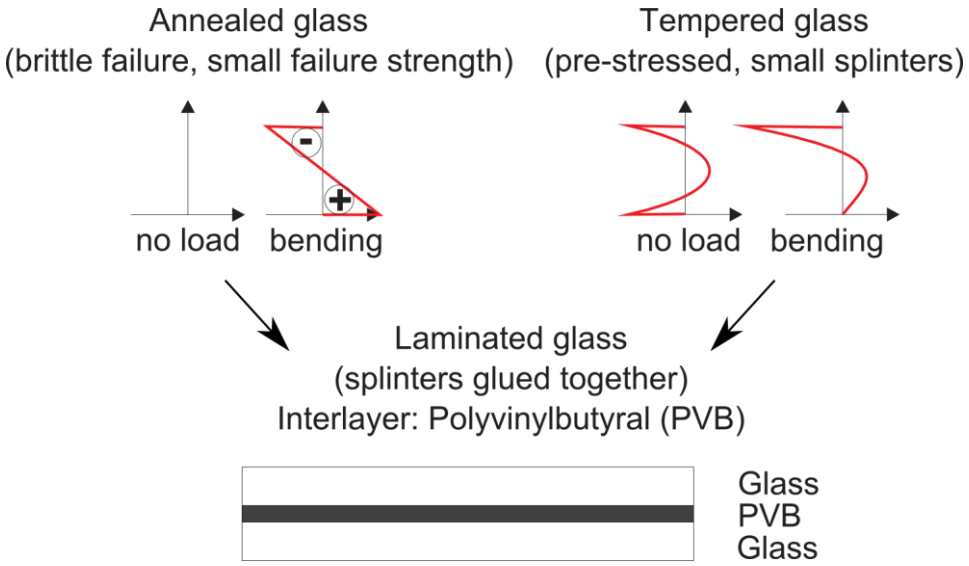

Figure 31: Main types of glass

5.3.3.1.1 Annealed Glass

This glass is cooled slowly in a controlled way in order to relieve internal stresses. The strength of this relatively inexpensive glass is small and the variation in strength is large. It is widely used for windows in cases where security against impact and blast is not important and where failure and the splinters produced do not affect human bodies (Dassault Systemes, 2012; Kinney et al., 1985; Kranzer et al., 2005; Beason et al., 1984; Overend et al., 2007; Brown 1974; Johnson et al., 1993).

5.3.3.1.2 Toughened Glass

Toughened glass or tempered glass is two or more times stronger than annealed glass. The production is done in such a way that residual stresses remain in the glass but in a manner that contribute to the increase of its bending strength. Both surfaces of the glass pane remain under compression, and when loaded by a pressure the induced tensile stresses are practically overcome by the existing residual compression, and thus the surface of the glass does not really enter in tension.

5.3.3.1.3 Heat-strengthened glass

Heat-strengthened glass is glass that has been heat treated in order to induce surface compression, but not to the extent of a tempered glass. The failure strength is therefore between the above two glass types.

5.3.3.1.4 Laminated Glass

Laminated glass is a combination of two or more glass sheets with one or more polymer inter-layers. Several types of laminated glass have been manufactured, with different types of glass materials, e.g. annealed glass and tempered glass, and with various inter-layers, such as polyvinyl-butyral (PVB) and SentryGlas®Plus. Laminated glass has the advantage that, following its failure due to blast loading, the produced fragments remain stuck to the interlayer, as graphically illustrated in Figure 32. Thus practically no splinters are formed and the risk of human injuries is contained. Three models can be adopted for calculating the response of laminated glass under air-blast loads, as shown in Figure 33.

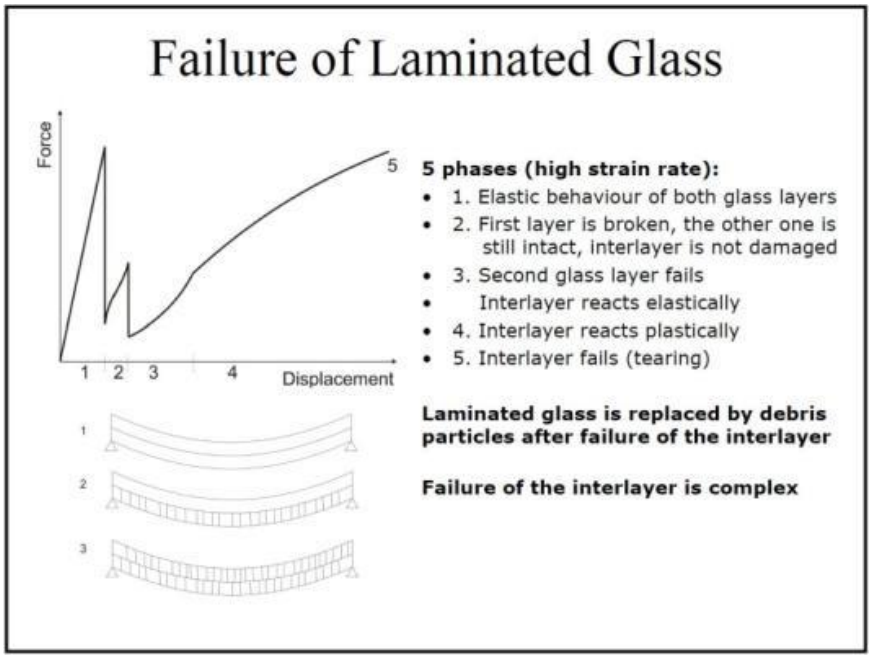

Figure 32: Phases of failure of laminated glass

a) **Layered elements with a special failure criterion**. After glass failure, the stresses are set to zero if the strains are greater than zero (tension) but the material can still react to compressive stress. If the inter-layer reaches the failure criterion of PVB, the element is eroded (Müller et al., 2008).
b) **Smeared model.** This is used to simulate post-failure behaviour (Timmel et al., 2007). Two coincident shells are used with two different material laws. The thickness, density and Young's modulus of these two shell elements are calculated in such a way that the combination of the two shell elements represents the behaviour of the sheet before failure. The behaviour of the laminate after failure of one of the glass plies is represented by only one of the shell elements.
c) **The 3D solid model.** This simulation requires very fine meshes, resulting in a long calculation time. The same material laws can be used as for layered shell elements. Some authors present 3D models with solid elements which allow using a detailed material law for the inter-layer (Wei et al., 2006; Bennison et al., 1999; Bennison et al., 2005).

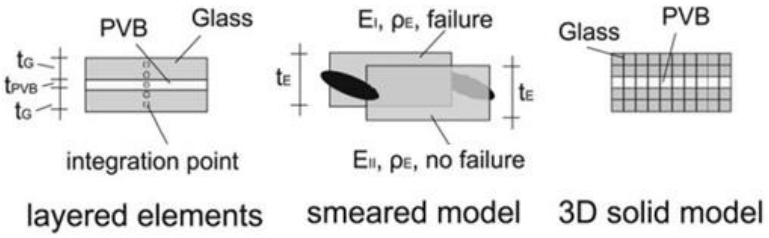

Figure 33: Models used for the simulation of laminated glass

Polyvinylbutyral (PVB). The long-time behaviour of PVB is visco-elastic, while the short-time behaviour is closer to elastic-plastic or brittle. Like other plastic materials, PVB shows failure at large strains (approximately 200 %), which indicates the need for a hyper-elastic material law. The Poisson ratio of the almost incompressible material is nearly 0.5, which can cause numerical problems if the material law is not adequately formulated.

The influence of large strains and large strain rates should be considered for blast- and impact-loaded laminated glass (Morison et al., 2007; Iwasaki et al., 2007; Bennison et al., 2005).

The behaviour of visco-elastic materials becomes more elastic-plastic below the glassy point. Since the behaviour of such materials under higher strain rates is often similar to the behaviour at lower temperatures, an elastic-plastic material law is just a first approximation. Further investigations should be done to identify the unloading behaviour of this material under higher strain rates (Du Bois et al., 2003; Sun et al., 2005).

The interfacial adhesion between the glass and the interlayer is produced by heating in combination with the application of high pressure. The mechanisms for the chemical adhesion depend on chemical and hydrogen bonding (Larcher et al., 2012). The gluing forces of PVB are relatively high, and de-bonding is not usually considered for blast-loaded laminated glass. An example of material data for the material parts of laminated glass is given in Table 6.

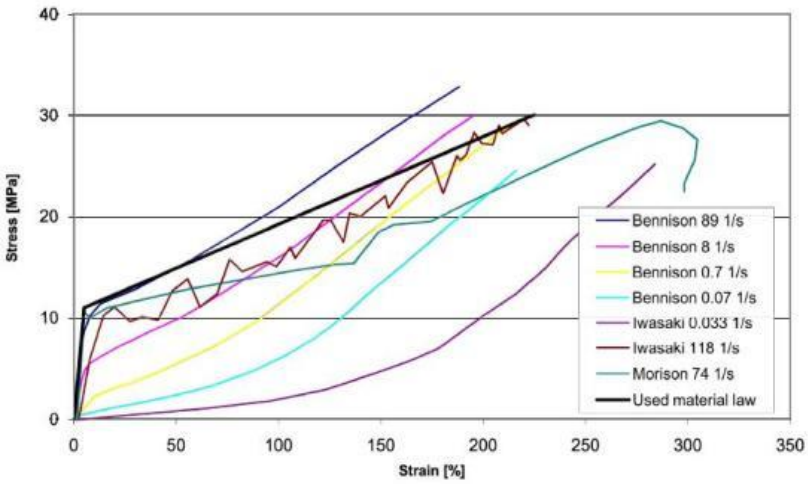

Figure 34: Behaviour of PVB at different strain rates

Table 6: Typical material properties for glass and PVB

Property	Glass	PVB
Initial Young's modulus [Pa]	7.0e10	2.2e8
Poisson ratio	0.23	0.45
Elastic limit [Pa]	-	11e6
Density [kg/m³]	2500	1100
Failure strain	0.0012	2
Failure stress [Pa]	84e6	28e6

5.3.3.2 Metallic Materials

Metallic materials like steel, iron, aluminium etc., constitute an important part of contemporary constructions. In the case of explosion events the deformations of the structural elements are very likely to enter the plastic domain and phenomena like strain hardening and material failure should be taken into account. Several models have been developed to describe the behaviour of metallic materials under severe dynamic loading conditions. The Ludwik model (Moras, 1999), the Cowper-Symonds model, the Armstrong-Zerilli model (Zerilli et al., 1987) and the Johnson-Cook model (Johnson et al., 1983) appear to be among the most commonly used ones.

5.3.3.2.1 Linear elastic behaviour

Typical metallic materials have elastic behaviour for small deformation. This behaviour is characterised by the fact that there is no residual deformation after loading. This behaviour is simulated using Young's modulus E and Poisson's ratio ν.

5.3.3.2.2 Johnson-Cook model

The Johnson-Cook model (Johnson et al.) is an empirical generalisation of the Ludwik's constitutive law, and expresses the true equivalent stress σ_{eq} in terms of the true equivalent plastic strain ε_{eq}^{pl} as:

$$\sigma_{eq} = \left(A_1 + A_2\left(\varepsilon_{eq}^{pl}\right)^{\lambda_2}\right)\left(1+\lambda_1 \ln\left(\frac{\dot{\varepsilon}_{eq}^{pl}}{\dot{\varepsilon}_{eq,\min}^{pl}}\right)\right)\left(1-\theta^m\right) \qquad (5.3\text{-}11)$$

where $\dot{\varepsilon}_{eq,\min}^{pl}$ is the minimum plastic strain-rate for which calibration has been made,

$$\theta = \frac{T - T_{room}}{T_{melt} - T_{room}} \qquad (5.3\text{-}12)$$

is the homologous temperature (T=temperature in Kelvin) and $A_1, A_2, \lambda_1, \lambda_2, m$ are five constants determined from fitting the model to experimental data (A_1 is the static yield stress). The form of this

function is related to the often made experimental observation that the increase of the flow stress is a logarithmic function of the strain rate.

5.3.3.3 Rubber Materials

In order for the laminated glass to be effective it needs to be strongly fixed to a supporting structure. If the joint or framing structure is not strong enough, the pane could get detached and enter the building at high velocity, injuring occupants. Structural silicone sealant is commonly used to bond the laminate to a framing structure. The laminate is restrained at two or four edges of the pane with a silicone bonded joint on one or both faces of the laminate. Securing all four edges on both sides is the recommended practice for blast resistance with a silicone joint of at least 35 mm in depth. There are also other methods of restraining laminated glass, such as rubber gaskets, glazing tape and mechanical point fixings. These systems are generally considered to give inferior blast protection to silicone bonded edges (Hooper, et al., 2012).
The elastic support of these rubber materials of the windows can be modelled by solid elements sharing some of the node elements of the laminated glass. The nodes at the top and at the bottom should be fixed. An elastic material law can be used with a Young's modulus of 3.5 MPa. However, the influence of the support fixing must be assessed by conducting parametric studies with different boundary conditions.

5.4 Engineering models

This chapter gives an introduction into the engineering method 'single degree of freedom model' (SDOF). This method tries to describe the global behaviour of structural elements which are exposed to extreme loads. Besides the finite element method (FEM), the SDOF method is an approach for the analysis of reinforced concrete, masonry and laminated glazing structures against extreme loading situations.

After a theoretical review of the SDOF method, the functionality of an engineering tool will be introduced shortly. These types of tools use SDOF models and calculate iso-damage curves for evaluating the resistance of building structures against blast loads.

The damage of structures loaded by detonations with large standoffs to the high explosive is characterised through a global response from the loaded structure (Chapter 2 of this document). The structure, or a large part of it, is loaded leading to a global response of the elements, such as bending. The SDOF method is widely used for the analysis, the prediction of damage and the design of structural elements loaded dynamically. An application is possible for calculating the structural response of elements against earthquake, explosions and impact (Bach et al., 2013).

The background of the SDOF-method is described in more detail in (Bach et al., 2013; Han et al., 1999; Sawcyk et al., 1963; Romani 2008; Fischer et al., 2009). The SDOF method is a widely used method to describe global loading processes and the related structural responses. The model is a simplification — only one degree of freedom is considered, as Figure 35 shows. The concept of SDOF comes from the necessity of solving equations of motion. The SDOF combines the response of a structural member to one-shape function $\phi(x)$ assuming the deflection shape function is known for the regarded element. Wherefore the displacement of the element, expressed through w(x,t), is described by only one degree of freedom. As Figure 35 indicates, motion in one direction is allowed.

The global displacement, expressed by Equation (5.4-1), depends on space and time. The time dependence is due to the change of the load during the time and inertia. A characterising pressure-time history of a blast load can be described through the Friedlander function (Equation 5.3-4), shown in Section 4.1, Figure 27:

$$w(x,t) = \phi(x)\, u(t) \tag{5.4-1}$$

$$p(t) = p_0 \left(1 - \frac{t}{t_+}\right) e^{-\left(A\frac{t}{t_+}\right)} \tag{5.4-2}$$

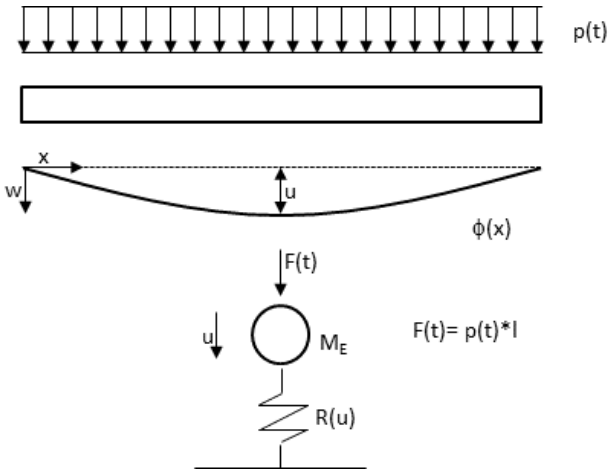

Figure 35: Simplification of a structural element loaded with a dynamic load (p(t)) to an SDOF model with its characterising properties (Bach et al., 2013)

The simplified model is shown below in Figure 35. The structural element is loaded through a characteristic pressure-time history p(t), leading to the deflection curve ϕ(x). The maximum deflection occurs in the middle of the element, and is denoted by u, where u=u(t) is a function of time.

The general equation of motion is shown in Equation 5.4-3 and by using the effective mass M_E in Equation 5.4-4 (Bach et al., 2013).

$$m\,\ddot{u} = \frac{1}{k_{LM}}\big(F(t) - R(u)\big) \tag{5.4-3}$$

$$M_E\,\ddot{u} = \big(F(t) - R(u)\big) \tag{5.4-4}$$

with F(t) the load applied on the structure, m the mass of the structure, R(u) its resistance and k_{LM} the load-mass factor. The load in the model is reduced to a single load F(t), as shown in Equation 5.4-5, with p(t) the pressure time history and l the element length.

$$F(t) = p(t)\, l \tag{5.4-5}$$

The loading scenario (p(t)) and the properties of the structural element are known. The exactness of the model is influenced by the determination of the resistance function (R(u)) of the structural member (Fischer et al., 2009). Numerical, analytical (Han, et al., 1999; Sawcyk, et al., 1963) experimental (Romani, 2008) and inverse (Fischer, et al., 2009) methods can lead to the material specific resistance function.

Based on a damage criterion, for example a critical deflection, this model can be implemented into a so-called engineering tool. With it an evaluation of the effects of a certain blast load on a structural element is possible. By comparing the pressure and positive specific impulse, characterising a blast load, with the resistance function of the structural element, a statement can be given whether the structural member is destroyed or not.

An example is shown in Figure 36. A resistance function is calculated for a certain structural element in a specific material and with specific dimensions. This information leads to the tool's result — a resistance function in the p-I-diagram, as shown in Figure 36.

An analysis of the damage of a structural element can be done through the comparison between reflected pressure and reflected impulse (certain blast load) to the calculated resistance function. If the point pressure/impulse lies above the resistance function, the structural member cannot resist the blast load. With this tool it is thus possible to make an evaluation of the blast resistance of structural elements produced in reinforced concrete, masonry and laminated safety glass.

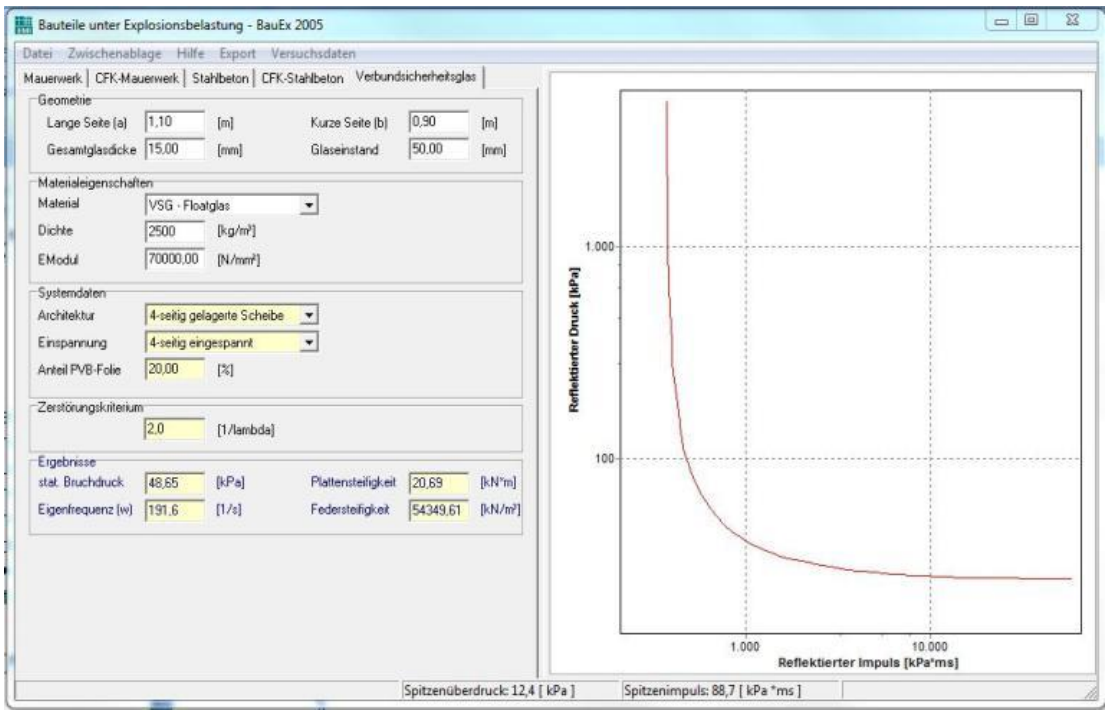

Figure 36: User interface of the engineering tool 'BauEx' and a resistance function in a p-I diagram for a specific structural element (right)

5.5 Verification and validation/error estimation

In order to get reliable numerical results calculation models and methods need to be verified against experimental data. In practice, first the reliability of the applied loading should be checked. Special attention should be paid in defining loading transients for near-field explosions. When the air is treated as a diatomic ideal gas, the assumption underestimates the reflected pressure.

Additionally strain rate-dependent material parameters are needed in order to simulate the material properties realistically. In many cases the assumed failure criteria is of crucial importance.

Verification/validation and error estimation is an important objective of all numerical simulations. In order to define a level of prediction of a numerical simulation, CEA (Commissariat à l'énergie atomique) developed a process called STANDARD V0.A (CEA). This procedure describes a way to validate each step of a simulation process in the field of weapon effects on structures. This procedure is based on the analysis and simulation of different explosive configurations (UFC, 2008; Baker, 1973; Kinney et al., 1985). Specific tests have been done in the past and have been used to evaluate simulation quality.
Each stage of a phenomenon is analysed:

- Detonation process;
- Blast wave propagation;
- Interaction with structure;

This document focuses especially on blast-wave generation and propagation to the structure but the way to analyse blast-wave validation can be transposed to the structure, too.

For each step, specific variables are checked. The principle variables are:

- Peak pressure of incident blast wave;
- Arrival time of blast wave;
- Positive impulse of incident pressure;
- Peak pressure of reflected blast wave;
- Positive impulse of reflected blast wave;

For each experiment, pressure sensors are located at different distances and duplicated at the same position in order to estimate the uncertainty of the measurement.

For specific experimental configuration (3D configuration) pressure sensors should be placed around the explosive in order to evaluate the shape of blast-wave propagation. Examples of sensors deployment are shown in Figures 37 and 38.

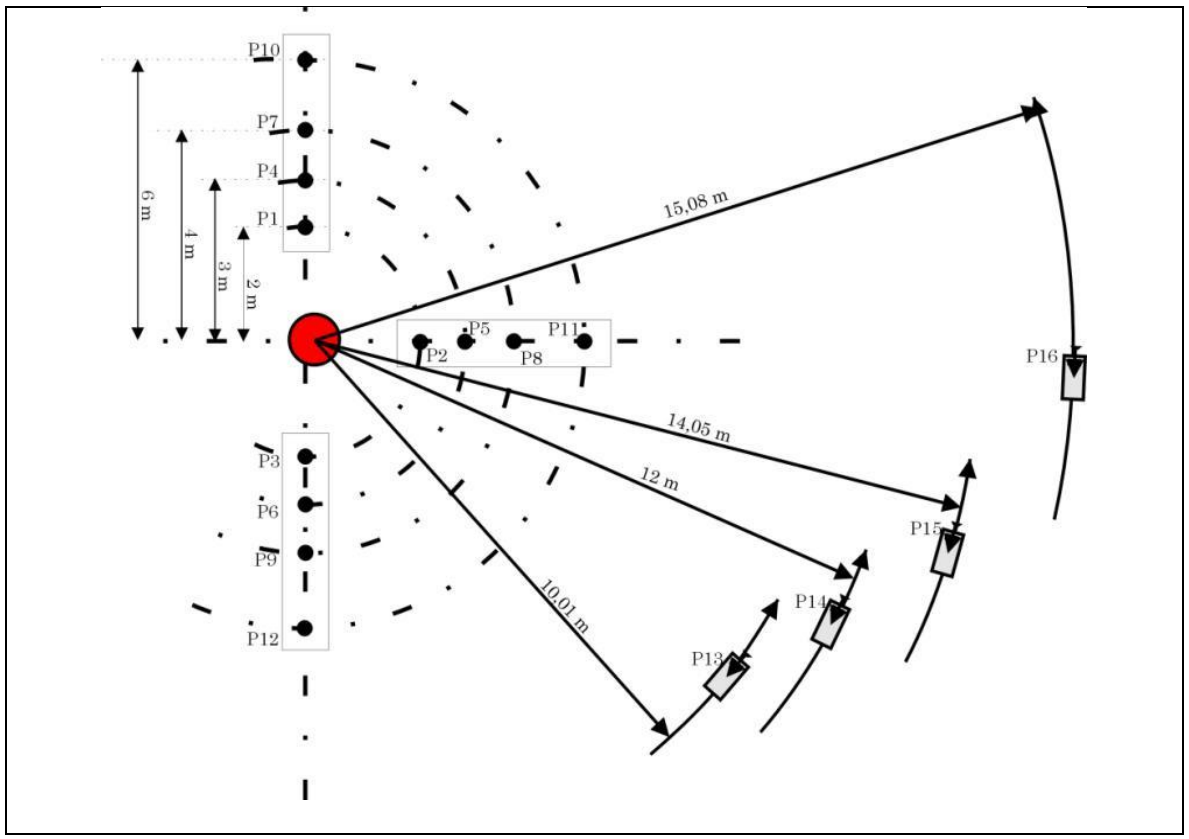

Figure 37: Typical experimental configuration for spherical charge detonation

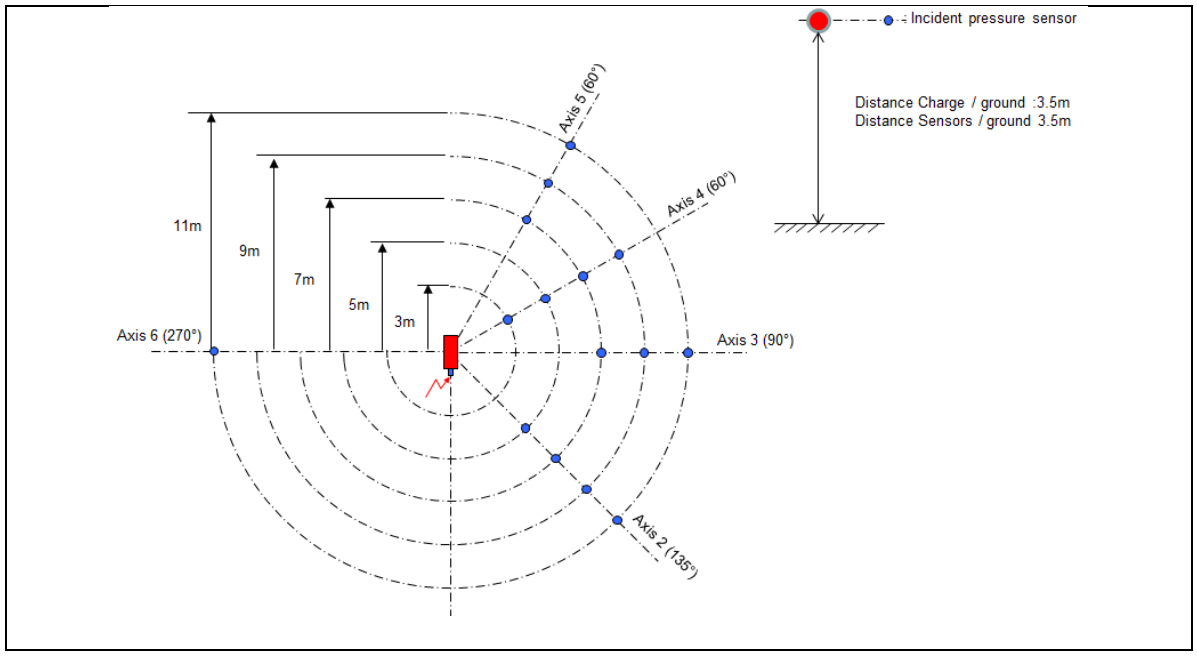

Figure 38: Typical experimental configuration for cylindrical charge detonation

The relative deviation of the simulated value of each specific variable (T_a, P_i, etc.) is obtained by the following formulas:

$$M\,\mathrm{arg}\,ing = \frac{V - V_{Exp\_moy}}{V_{Exp\_moy}} \tag{5.5-1}$$

with

$$V_{Exp\_moy} = \frac{1}{N_{test}} \sum_{i=1}^{N_{test}} V_i \tag{5.5-2}$$

where, V = Simulation variable value

V_{Exp_moy} = Mean arithmetic experimental value

V_i = Experimental value

N_{test} = Number of same test measurements

The simulation process of blast-wave propagation is considered as satisfactorily simulated when each specific variable is calculated with a difference from $V_{exp,Moy}$ of less than 5 % (when the scattering experimental value is less than 10 %).

To reach this validation process, different parameters should be used.

- Equation of state for explosive and air modelling;
- Mesh size;
- Numerical parameter (pseudo-viscosity);
- etc.

A convergence criterion is used to define the minimum size Δx of the elements during the simulation process. Based on the literature, a specific mesh size Δx_{ref} has been defined to simulate blast-wave propagation generated by detonating a reference mass of M_{ref}=175.5 kg spherical charge (ambient condition: 1.013 bars, 20 °C).

$$\Delta x \le \Delta x_{ref} \cdot \sqrt[3]{\frac{M}{Mref}} \tag{5.5-3}$$

Similitude formulas (specific for a spherical charge) are used for the reduction of the experimental and simulation data and for plotting them in the same graph:

$$Z = \frac{D}{M^{1/3}} \tag{5.5-4}$$

with Z = Scaled (or normalised) distance (m/kg$^{1/3}$)

D = Stand-off distance (m)

M = Explosive weight (kg)

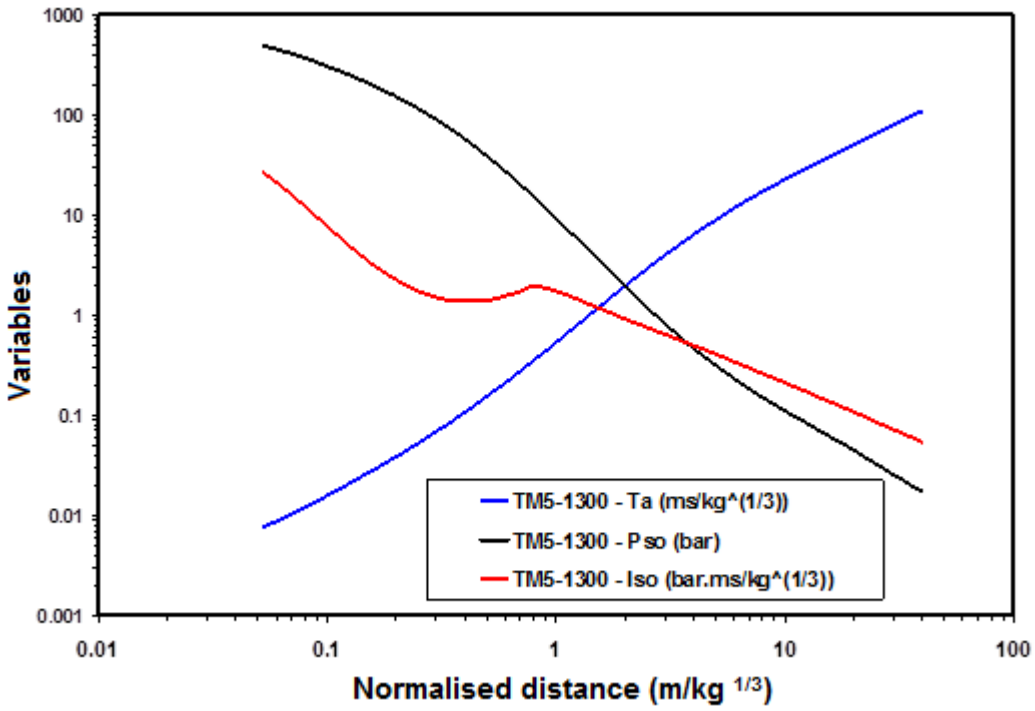

Figure 39: Variables T_a (arrival time), P_{so} (peak side-on incident pressure) and I_{so} (incident impulse) as functions of normalised distance

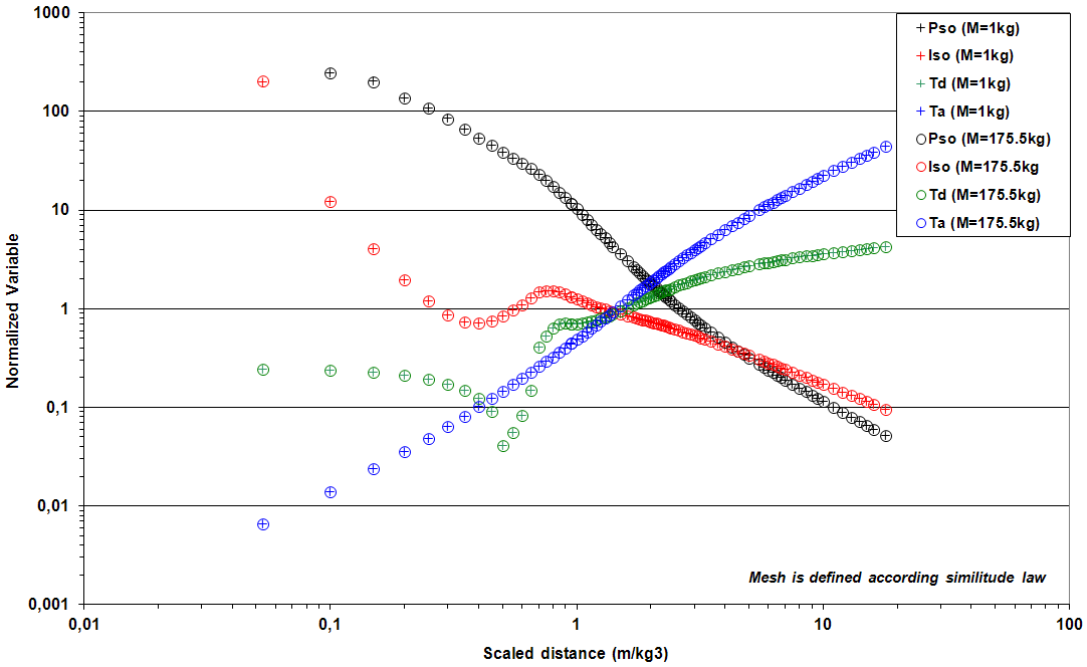

Figure 40: Variables T_a, P_{so} and I_{so} as functions of the normalised distance, spherical charge with 175 and 1 kg of TNT

The similitude law produces equations for the several variables, which written for ambient pressure, are:

$$\text{Space: } Z = \frac{D}{M^{1/3}}; \quad \text{Time: } \bar{t} = \frac{t}{M^{1/3}}; \quad \text{Pressure: } \bar{P} = P; \quad \text{Impulse: } \bar{I} = \frac{I}{M^{1/3}} \qquad (5.5\text{-}5)$$

A relevant graph from the available empirical analytical relationships (UFC, 2008) is given in Figure 39. Thanks to this methodology, it is possible to represent different explosive masses if the mesh size follows Equation 5.5-3. As an example and for comparison purposes, results of simulations with 175 kg and 1 kg of TNT spherical charges are presented in Figure 40.

All the above procedures have been applied in (CEA), defining a matrix of limit values for simulation validity in a specific configuration:

Table 7: Matrix of simulation validity for a specific blast configuration

Configurations	Time	Pressure	Impulse
Aerial explosion of spherical charge abacus[(1)]	*±5 %*	*±18 %*	*±15 %*
Aerial explosion of hemispherical charge CEA GRAMAT Test[(1)]	*±4 %*	*±11 %*	*±13 %*
Aerial explosion of cylindrical charge [(1)]	*±4 %*	*±11 %*	*±13 %*
Aerial explosion of spherical charge and Mach stem [(2)]	*±4 %*	*±11 %*	*±13 %*
Internal explosion of spherical charge[(2)]	*±4 %*	*±20 %*	*±15 %*
Global criterion	***±5 %***	***±20 %***	***±15 %***

[(1)]Incident blast wave: Time=Ta; Pressure=Pso and Impulse=Iso

[(2)]Reflected blast wave: Time=Tr; Pressure=Pr and Impulse=Ir

After the blast-wave simulation process, it is necessary to evaluate the response of the structure and the corresponding error. The same protocol should be applied, based on the definition of the specific variable representing structural deformation. Typical parameters to be considered are:

- Displacement;
- Maximum stress and strain;
- Failure.

Defining the critical pressure for a specific structure leads to defining the critical distance at which the structure will not survive. Based on the analysis described before, it is possible to determine the critical position of an explosive with an error bar indicating the level of confidence in the simulation. An application on structural vulnerability is shown in Figure 41.

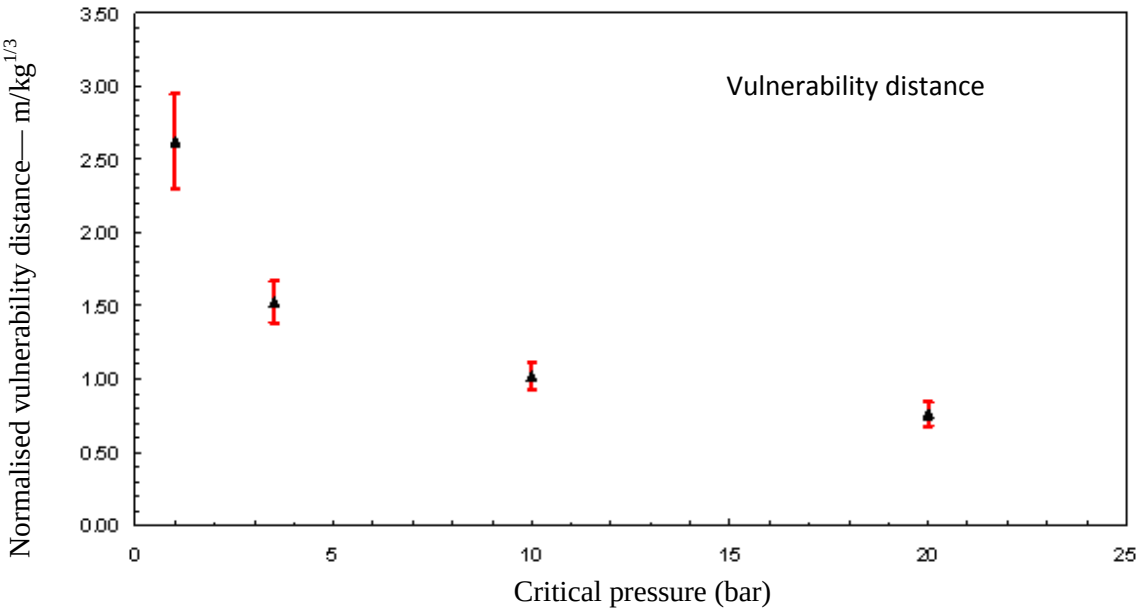

Figure 41: Influence of simulation restitution on vulnerability distance

5.6 List of references

Abaqus 2012. Abaqus version 6.12 manual, Dassault Systems.

Dobratz B.M, Crawford P.C 1985. LLNL Explosives Handbook: Properties of Chemical Explosives and Explosive Simulants, Lawrence Livermore National Laboratory, UCRL-52997, Lawrence Livermore Laboratory, Berkeley.

CEN, 2001. EN 13123-1: Windows, Doors and Shutters — Explosion Resistance — Requirements and classification — Part 1: Shock Tube.

Kinney G. F, Graham K. J 1985. Explosive shocks in air. Second edition. Springer Berlin.

Kranzer C, Gürke G, Mayrhofer C. 2005. Testing of bomb resistant glazing systems. Experimental investigation of the time dependent deflection of blast loaded 7.5 mm laminated glass. In: Glass processing days.

Beason, W.L, Morgan, J.R. 1984. Glass failure prediction model. Journal of Structural Engineering, 110 (2), pp. 197-212.

Overend M, Parke G.A.R, Buhagiar D, 2007. Predicting failure in glass – A general crack growth model. Journal of Structural Engineering, 133(8), pp. 1146-1155.

Brown WG. 1974. A Practicable Formulation for the Strength of Glass and Its Special Application to Large Plates. Publication No. NRC 14372, National Research Council of Canada, Ottawa.

Johnson, G.R, Holmquist, T.J 1993. An improved computational constitutive model for brittle materials, Joint AIRA/APS Conference, Colorado Springs, Colorado, June 1993.

Müller R, Wagner M. 2008. Berechnung sprengwirkungshemmender Fenster- und Fassadenkonstruktionen. Bauingenieur; 81(11):475-87.

Timmel M, Kolling S, Osterrieder P, Du Bois P. 2007. A finite element model for impact simulation with laminated glass. International Journal of Impact Engineering; 34:1465-78.

Wei J, Dharani L. 2006. Response of laminated architectural glazing subjected to blast loading. International Journal of Impact Engineering; 32:2032-47.

Bennison S.J, Jagota A, Smith C.A 1999. Fracture of glass/poly(vinyl butyral) (butacite) laminates in biaxial flexure. Journal of the American Ceramic Society; 82(7):1761-70.

Duser A.V, Jagota A, Bennison S.J 1999. Analysis of glass/polyvinyl butral laminates subjected to uniform pressure. Journal of Engineering Mechanics; 125(4):435-42.

Morison C, Zobec M, Frenceschet A 2007. The measurement of PVB properties at high strain rates, and their application in the design of laminated glass under bomb blast. In: ISIEMS 2007, International symposium on interaction of the effects of munitions with structures, 17-21 September 2007, Orlando, US.

Iwasaki R, Sato C, Lataillade JL, Viot P 2007. Experimental study on the interface fracture toughness of PVB (polyvinyl butyral)/glass at high strain rates. International Journal of Crashworthiness; 12(3):293-8.

Bennison S, Sloan J, Kistunas D, Buehler P, Amos T, Smith C 2005. Laminated glass for blast mitigation: role of interlayer properties. In: Glass processing days.

Du Bois PA, Kolling S, Fassnacht W 2003. Modelling of safety glass for crash simulation. Computational Materials Science; 28(3e4):675-83.

Sun D, Andrieux F, Ockewitz A, Klamser H, Hogenmüller J 2005. Modelling of the failure behaviour of windscreens and component tests. In: 5th European LSDYNA Users Conference, 25-26 May, 2005.

Larcher M, Solomos G, Casadei F, Gebbeken N 2012. Experimental and numerical investigations of laminated glass subjected to blast loading. Int. J. Impact Engineering (39) 42-50.

Moras B, 1999. Constitutive Equations of Strain Rate Sensitive Materials for the Automotive Industry. PLEXIS-3C Implementation Report, JRC Technical Note N. I.99.54.

Johnson G.R, Cook, W.H, 1983. A constitutive model and data for metals subjected to large strains, high strain rates and high temperatures, Proceedings of the 7th International Symposium on Ballistics: 541–547.

Zerilli F.J, Armstrong R.W, 1987. Dislocation-Mechanics-Based constitutive relations for material dynamics calculations, Journal of Applied Physics, (61), pp. 1816-1825.

Hooper P.A, Sukhram R.A.M, Blackman B.R.K, Dear J.P, 2012. On the blast resistance of laminated glass, International Journal of Solids and Structures, (49) pp. 899-918.

Peroni M, Solomos G, Pizzinato V, Larcher M, 2011. Experimental investigation of high strain-rate behaviour of glass. Applied Mechanics and Materials, (82) 63-68.

Bach A, Stolz A, Nöldgen M, Thoma K, 2013. Modelling of preloaded reinforced-concrete structures at different loading rates, 2013 VIII International Conference on Fracture Mechanics of Concrete and Concrete Structures.

Han S.M, H. Benaroya H, et al. 1999. Dynamics of transversely vibrating beams using four engineering theories. Journal of Sound and Vibration. 255(5): pp. 935-988.

Sawcyk A, Jäger T, 1963. Grenztragfähigkeitsanalyse der Platten, Berlin, Springer.

Romani M, 2008. Mauerwerk unter Druckstoßbelastung - Tragverhalten und Berechnung mit Verstärkung durch Kohlefaserlamellen. Universität BW München.

Fischer K, Häring I, 2009. SDOF response model parameters from dynamic blast loading experiments. Engineering Structures, 21(8): pp. 1677-1686.

CEA: Standard OURANOS V0.A EFFET DES ARMES, RESTRICTED.

Unified Facilities Criteria UFC 3-240-02, 2008. Structures to Resist the Effects of Accidental Explosions, US Department of Defense, US Army Corps of Engineers, Naval facilities Engineering Command, Air Force Civil Engineer Support Agency – 5 December 2008 (replaces ARMY TM5-1300 of November 1990).

Baker W.E 1973. Explosions in Air, University of Texas.

List of Tables

List of Figures

European Commission
EUR 26449 EN – Joint Research Centre – Institute for the Protection and Security of the Citizen (IPSC)

Title: Resistance of structures to explosion effects: Review report of testing methods
Authors: Kevin C., Ans van Doormaal, Christof Haberacker, Götz Hüsken, Martin Larcher, Arja Saarenheimo, George Solomos, Alexander Stolz, Laurent Thamie, Georgios Valsamos

Luxembourg: Publications Office of the European Union

2013 – 78 pp. – 21.0 x 29.7 cm

EUR – Scientific and Technical Research series – ISSN 1831-9424

ISBN 978-92-79-35104-4

doi:10.2788/57271

Abstract

IIt is important to protect critical buildings (shopping centres, government buildings and embassies), infrastructure and utilities, train and underground stations against being damaged, destroyed or disrupted by deliberate acts of terrorism, criminal activity and malicious behaviour. Normal regulations and building guidelines do not generally take into account these threats. The introduction of regulations or guidelines should support the resilience of the buildings and infrastructure against explosive incidents.
In order to protect the infrastructure, methods are required to quantify the resistance of structural elements against explosive loading and to assess the hazards resulting from failure of an element. The applicable state-of-the-art techniques may be either experimental or numerical methods, or a combination of both.
Therefore, the thematic group (TG) on the resistance of structures to explosion effects was formed in order to bring the required expertise together, make it commonly available and to find and define harmonised methods and solutions which can be provided to the decision-makers responsible for critical infrastructure protection. This first report of the TG gives a comprehensive summary of the existing methods which can be used to analyse and test the resistance of glazing and windows under blast-loading conditions.
Within this context, the experimental methods of testing using high explosives and testing using blast simulators called shock tubes is presented and explained. In addition, the potential of numerical simulations is highlighted in terms of their applicability to the different glass materials.
A short, comprehensive theoretical background is given for each method. Based on this, each method is described with its requirements, realisation and the related measurement techniques. Furthermore, an interpretation of the measurements is highlighted.
For the numerical simulations, the basic discretisation and calculations schemes are presented in combination with the available constitutive material descriptions for the different significant materials. Finally the chances for verification and validation of the numerical results are presented.
Hence the report builds the basis for an actual evaluation of the different test methods and their applicability to certain problems, and provides helpful information for critical infrastructure stakeholders, owners and operators considering the structural resistance of the infrastructure to the effects of explosion in a comprehensive document.

LB-NA-26449-EN-N

As the Commission's in-house science service, the Joint Research Centre's mission is to provide EU policies with independent, evidence-based scientific and technical support throughout the whole policy cycle. Working in close cooperation with policy Directorates-General, the JRC addresses key societal challenges while stimulating innovation through developing new methods, tools and standards, and sharing its know-how with the Member States, the scientific community and international partners.

Publications Office

ISBN 978-92-79-35104-4